Chapter 3

Dynamics of lunar meteoroids

3.1 Introduction

Three decades ago Arnold (1965) and Wetherill (1968) used Monte Carlo simulations to investigate the expected 4π cosmic ray exposure ages (CREs) of lunar meteorites. These authors each found that a steep spectrum of exposure ages should be expected, with the bulk of the objects having 4π CREs < 1 Myr. While lunar meteorites were not actually present in the collection at that time, the age spectrum of the available meteorites combined with the asymmetry in the time of fall (Wood 1961, Wetherill 1968) was largely able to rule out the Moon as a source of much meteoritic material. More recently, Gault (1983) performed some short-term simulations of the geocentric evolution of ejected lunar material showing that most material escaping the Moon is ejected to heliocentric orbit.

Information is also available on micrometeoroid streams (*e.g.,* Svedhem *et al.* 1994) observed in the near-Earth environs. These micrometeoroids have sometimes been hypothesized to be particles of lunar ejecta (see, for example, Dohnanyi 1977). Since the interpretation of these data is quite complex and few firm conclusions can be drawn, I will not consider this topic further.

3.2 Numerical Simulations of lunar ejecta

The Moon is bombarded by a variety of projectiles. The nature of the impactors is not important for our purposes, whether they be 'normal' Earth-crossing asteroids or comets (see discussion in Chpt. 6). I take as incontrovertible that, following impact, some impactors produce a (likely very small) fraction of ejecta fragments that reach speeds above the lunar escape velocity. The relevant acceleration

[*] This chapter is based on the paper: Gladman, B., J.A. Burns, M. Duncan, and H. Levison (1995), The Dynamical Evolution of Lunar Impact Ejecta, *Icarus* **118**, 302–321 [copyright 1995 by Academic Press, Inc.]

Table 3.1 Initial conditions for the Sun, Earth, and Moon used in the geocentric stage simulations. Masses are in solar masses, lengths in AU, and the unit of time is the mean solar year divided by 2π. The origin is at the 3-body barycenter.

Geocentric Initial Conditions			
	Sun	Earth	Moon
M	1.00000000	3.040438×10^{-6}	3.7536×10^{-8}
x	-0.00000051445068	0.16716510695187	0.16505548128342
y	0.00000298358568	-0.96935160427807	-0.96792780748663
z	-0.00000000034939	0.00011399064171	0.00007492647059
v_x	-0.00000308328240	1.00194735428418	0.98368251410153
v_y	-0.00000053203717	0.17321044856299	0.14390276658609
v_z	0.00000000005244	0.00002041304056	-0.00305048683857

mechanism is uncertain, and not important to this work; both a shock-wave interference model (Melosh 1984) and a vapor-plume acceleration model (O'Keefe and Ahrens 1986) have been proposed. In either case one expects a spectrum of sizes and velocities produced for the ejecta, with the number of launched objects decreasing rapidly with increasing velocity (Gault 1963, Vickery 1987, Frisch 1992). Thus it is likely that most escaping ejecta will leave the Moon's surface barely above the lunar escape velocity of 2.38 km/s ($= \sqrt{2GM_m/R_m}$, with G being the gravitational constant, M_m and R_m the lunar mass and radius, respectively), neglecting three-body effects. The question that will be addressed here is: what is the fate of these objects once they are ejected from the lunar surface and have escaped into geocentric orbit?

A first approach might be to model the particle, Earth, and Moon within the context of a circular restricted three-body problem. This level of approximation is surely too extreme since the Moon's orbital radius of 60 $R_\oplus$ is an appreciable fraction of the radius of the Earth's Hill sphere with respect to the Sun (which is about 230 $R_\oplus$). Thus, even mild increases in the ejecta's apogee, caused by the particles scattering off the Moon's gravitational field, allow their orbits to be strongly perturbed by the Sun even before the particles become unbound from geocentric orbit.

To improve on the three-body model, I undertook a full four-body treatment, with a massless test particle moving under the effect of the Sun, Earth, and Moon; the JPL ephemerides were used to construct initial conditions for the three massive objects, all having their correct relative orbits (Table 3.1). Some details on the method used in the geocentric integrations are presented in the next section. This model should be sufficiently valid during the brief interval that the meteoroid remains in geocentric orbit (called the 'geocentric stage'). Since the particles escape to heliocentric orbit rather quickly (taking typically much less than a few decades), the effects of the other planets on the fragment's evolution in this stage are negligible. However, in this geocentric phase the Moon's presence is critical to the orbital evolution. Once the particle reaches heliocentric space (*i.e.,* the heliocentric stage) a different model is necessary (see section 3.2.2).

3.2.1 Geocentric Phase

I have conducted a large number of simulations of impact ejections off the lunar surface. For each simulation 20 (sometimes 40 or 60) random impact sites were distributed over the lunar surface, weighted so that each unit area was equally likely. For our purposes, a uniform impact distribution is a good approximation; the Earth has little influence as a shield or a focus (see Bandermann and Singer 1973). From each site 18 particles were launched at 45° relative to the surface (Melosh 1989) and spaced evenly in local azimuth (Fig. 3.1).

In each simulation all particles have a common launch speed, with values ranging from 2.3 to 3.5 km/s. While the large number of events should provide a statistical view of the probable fates of most lunar fragments, launch speed is the single most uncertain parameter for this study. This is especially important because, as shown below, the fraction of particles that impact the Earth during the geocentric phase depends strongly on the launch velocity. I believe that the 2.4 km/s case is the most relevant to study since it is quite likely that the number of objects decreases quite rapidly as a function of launch speed; thus the largest number of escaping particles will do so at just above the escape speed (see Burns *et al.* 1984 and Wetherill 1984 for discussions and relevant references).

While a 45° ejection angle may characterize crater excavation flows (Melosh 1989), a spallation process may produce typical ejection angles that are somewhat different (Frisch 1992); similarly the distribution of ejecta masses and velocities may differ. A change in ejection angle will simply alter the direction of the residual velocity vector (defined below), and should have no effect on the results since a large number of impacts have been studied.

After ejection, the particles' orbits are evolved using a sixth-order explicit symplectic integration algorithm (see Gladman *et al.* 1991) using the full 4-body equations of motion. The particles are followed until they impact the Earth or Moon, or they escape to heliocentric orbit. After reaching 10 Hill sphere radii from the Earth (whose Hill radius is $\simeq 0.01$ AU) the particles have their heliocentric orbital elements computed in order to transfer them to the heliocentric stage simulation (Sec. 3.2.2).

The integrator is a brute-force method which simply evaluates the interparticle forces and integrates Newton's equations. Therefore, each of the four particles are given a mass and radius (the test particle has negligible mass and size) as well as initial position and velocity vectors. The algorithm advances the particles forward one time step, detecting collisions by monitoring the relative distance of

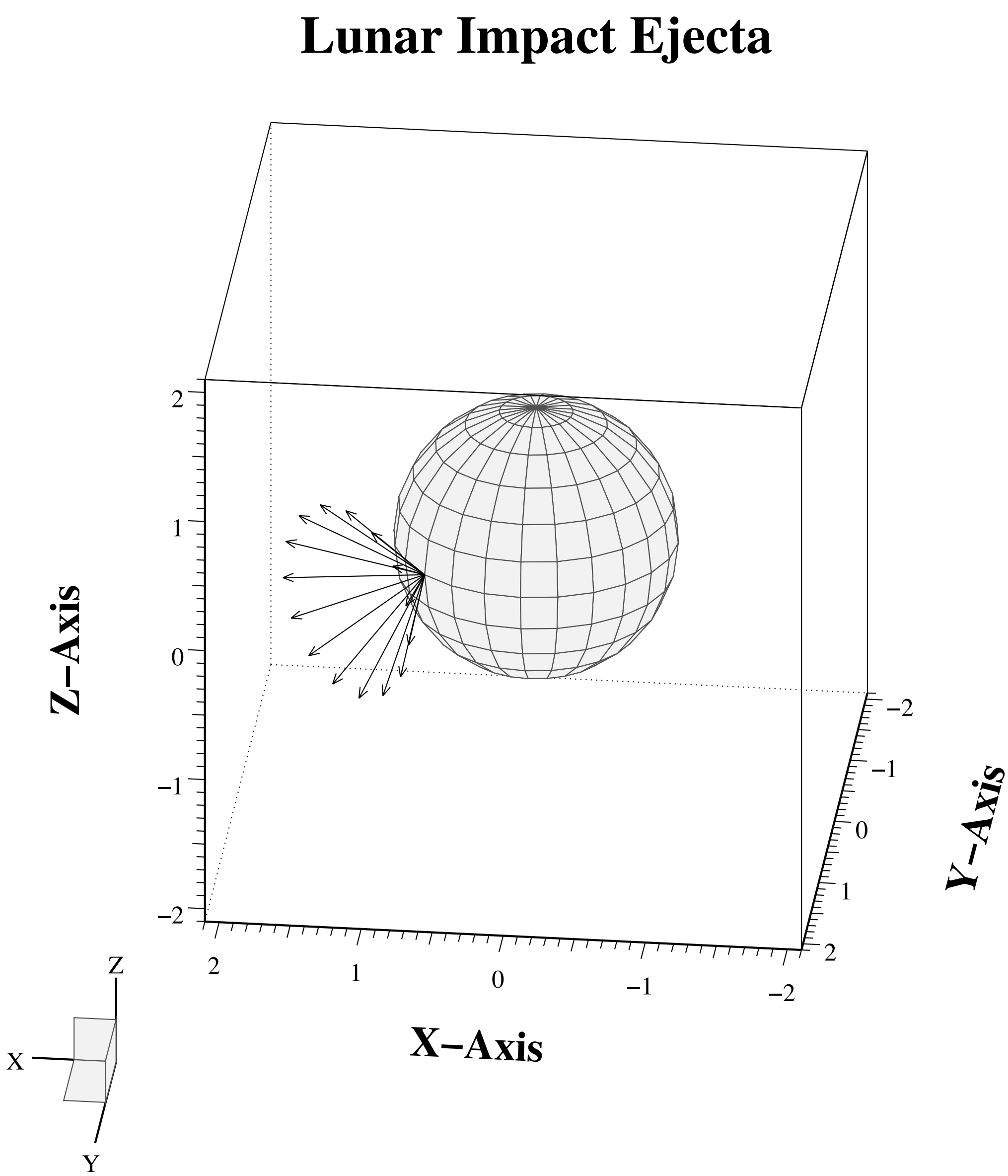

Figure 3.1 The initial velocity vectors of particles launched from a single lunar impact. Impact sites are chosen randomly on the surface of the Moon (equally probable per unit area). From each site 18 particles are ejected, spaced equally in azimuth on a cone of 45^o opening angle (only 15 vectors are shown, for clarity). In this figure the positive X axis points in the direction of the Moon's motion, the positive Y axis points towards the Earth, and the scales are in lunar radii. All particles are launched with a common speed.

the small particle from the Earth and Moon. Since the CPU time required for the geocentric integrations is relatively small, I have used a time step (of 0.04 hours) small enough that the truncation error is below the machine precision (of $\sim 10^{-16}$) for the integration of the Moon's orbit. I have handled close approaches to the Earth and Moon by simply lowering the time step, and insured that the (statistical) results have no dependence on the time step.

Due to the large number of papers in the literature that attempt to establish links between certain meteorites and their launch locations I will spend considerable time discussing the details of the geocentric dynamics. The casual reader may wish to skip to the final paragraph of section 3.2.1 (p. 30) at this point.

Table 3.2 shows the outcomes of the geocentric simulations as a function of the launch speed from the lunar surface. For several launch speeds, more than one simulation was performed; this gives us some estimate of the sampling error due to a finite number of impact sites and launch azimuths. The gross histories of these particles are relatively easy to understand. At $v_l = 2.4$ km/s, particles are barely above the lunar escape speed and by the time they have reached several tens of lunar radii, almost all of their launch velocity (relative to the Moon) is gone; thus they share the nearly circular lunar orbit with its 1 km/s geocentric velocity. Such particles will suffer many strong repeated scatterings by the Moon. (Note that my qualitative discussions, but not the simulations, of the dynamics ignore the complexities of the Moon's eccentric and inclined orbit; these 5% effects are unimportant to a general understanding of the dynamics.)

Interestingly, the Moon is unsurpassed by other planetary satellites (except for Charon) in its ability to scatter particles that share similar orbits. The power of the Moon in this regard can be easily understood. The mean lunar orbital velocity is $\simeq 1$ km/s, while the Moon is capable of providing a maximum gravity assist (in a surface-skimming close encounter) of $v_{esc}/\sqrt{2} \simeq 1.7$ km/s. Thus the Moon can cause major changes in the geocentric orbital elements of particles in orbits similar to its own; indeed a single close encounter can be sufficient to eject particles from geocentric orbit. In fact, approximately 15% of the initially launched particles receive their 'gravity assist' out of geocentric orbit *during* their initial escape from the Moon; these particles make up the apparent clump near $a \simeq 1.05$ AU, $e \simeq 0.045$ to be seen later in Fig. 3.6; this interesting phenomenon is further explored in Appendix A. Compared to the number of particles that escape to heliocentric space, relatively few will suffer the fortuitous chain of events that walk their perigees down to the Earth's radius. The roughly 3% that do impact the Earth via this mechanism all require many months (to a few years) and several strong lunar perturbations to do so. It is much more likely that they will receive a perturbation that ejects them, although $5 - 10\%$ recollide with the Moon during this process. (Since the initial orbits are similar to the Moon's, the encounters occur at low relative velocity, which enhances the Moon's gravitational cross section.) For higher launch velocities, lunar re-impacts become very rare.

Table 3.2 For each geocentric-stage simulation (in which all particles are launched from the Moon at a single launch speed v_l), the table lists the total number N of particles launched (18 particles per impact site), the percentage Esc of particles that escape to heliocentric space, and the percentages that impact the Earth ($\oplus$) and Moon (M). The five simulations marked * were used as initial conditions for the heliocentric simulations.

Geocentric Stage Results				
v_l (km/s)	N	Esc(%)	% $\oplus$	% M
2.3	360	0.0	0.0	100.0
2.4	360	88.1	3.3	8.6
2.4	360	91.7	3.9	4.4
2.4	360	90.0	3.3	6.7
2.4	720	91.1	2.2	6.7
2.4*	360	90.5	3.1	6.4
2.5	360	92.8	5.5	1.7
2.6	360	80.0	18.9	1.1
2.6	720	83.7	16.0	0.3
2.6*	360	81.7	18.0	0.3
2.8	360	81.4	18.1	0.5
2.8	360	77.2	22.5	0.3
2.8*	360	80.2	19.2	0.6
3.0	360	95.3	3.9	0.8
3.0*	360	94.7	5.0	0.3
3.2	360	100.0	0.0	0.0
3.2	1080	99.3	0.7	0.0
3.2*	360	99.1	0.6	0.3
3.5	360	100.0	0.0	0.0

Fig. 3.2 shows the evolution for a typical particle escaping at 2.4 km/s; note the almost-circular initial orbit and the many lunar close encounters.

In each simulation all particles have a common launch speed, with values ranging from 2.3 to 3.5 km/s. To help interpret the results in Table 3.2, let us for the moment ignore the presence of the Earth and Sun, and study particles as they escape the lunar gravitational field (Fig. 3.3). Far from the Moon the particles will retain some 'residual velocity' $\vec{\boldsymbol{v}}_{\boldsymbol{r}}$ which is measured with respect to the (moving) Moon. The magnitude and direction of $\vec{\boldsymbol{v}}_{\boldsymbol{r}}$ will differ depending on launch speed, site, and direction; furthermore, the final orientation of $\vec{\boldsymbol{v}}_{\boldsymbol{r}}$ will be influenced by the bending of the trajectory that occurs as the particle escapes from the lunar field. By considering the geometry of the outgoing hyperbolic orbits one can show, for a 45^o ejection, the angle (in radians) that the path is deflected from its initial launch direction (see Fig. 3.3a) to be:

$$\delta(v_l) = \arccos\left(\frac{-1}{\sqrt{x^2 + (x-1)^2}}\right) + \arctan\left(\frac{x-1}{x}\right) - \frac{3\pi}{4}, \tag{3.1}$$

where the square root of x is the dimensionless ratio of the launch speed to the lunar escape speed ($x \equiv v_l^2 R_m / 2GM_m$); relation (3.1) is plotted in Fig. 3.3b. In agreement with one's intuition, particles launched at high speeds are scarcely turned by the Moon's gravity while the trajectories of those thrown at near the escape speed are pulled significantly away from the local vertical.

Once free of the lunar gravitational field, the residual velocity vector will have a magnitude of roughly

$$v_r \simeq \sqrt{v_l^2 - (2.38 \text{ km/s})^2} \tag{3.2}$$

from conservation of energy, again ignoring the complexities of three-body effects. As will now be discussed, the particle's fate is largely determined by the 'escape angle' θ between $\vec{\boldsymbol{v}}_{\boldsymbol{r}}$ and the Moon's velocity vector $\vec{\boldsymbol{v}}_{\boldsymbol{m}}$ at the time of escape from the lunar gravity field.

To estimate the initial *geocentric* velocity $\vec{\boldsymbol{v}}_{\boldsymbol{i}}$ that appears in the four-body integration, consider the following idealization: the residual component is added vectorially to the lunar orbital velocity $\vec{\boldsymbol{v}}_{\boldsymbol{m}}$ of magnitude $\simeq 1.0$ km/sec to obtain $\vec{\boldsymbol{v}}_{\boldsymbol{i}}$, as shown in Fig. 3.3a. The angle θ between $\vec{\boldsymbol{v}}_{\boldsymbol{r}}$ and $\vec{\boldsymbol{v}}_{\boldsymbol{m}}$ will be called the 'escape angle' and is very important in determining the potential fate of the escaping particles. For a given v_r the fastest (i.e., largest v_i) escaping ejecta will clearly have $\theta = 0$; such particles do not originate from the leading point of the Moon (because the ejecta there are launched at 45^o from the lunar motion), nor from an annulus 45^o away from the leading point (because such particles still suffer deflection unless $x \gg 1$). Instead, the fastest ejecta originate on an annulus $(45+\delta)^o$ away from the leading point and, even then, only on the small portion of the ejection cone that points parallel to the lunar motion. Similarly, the *slowest* initial

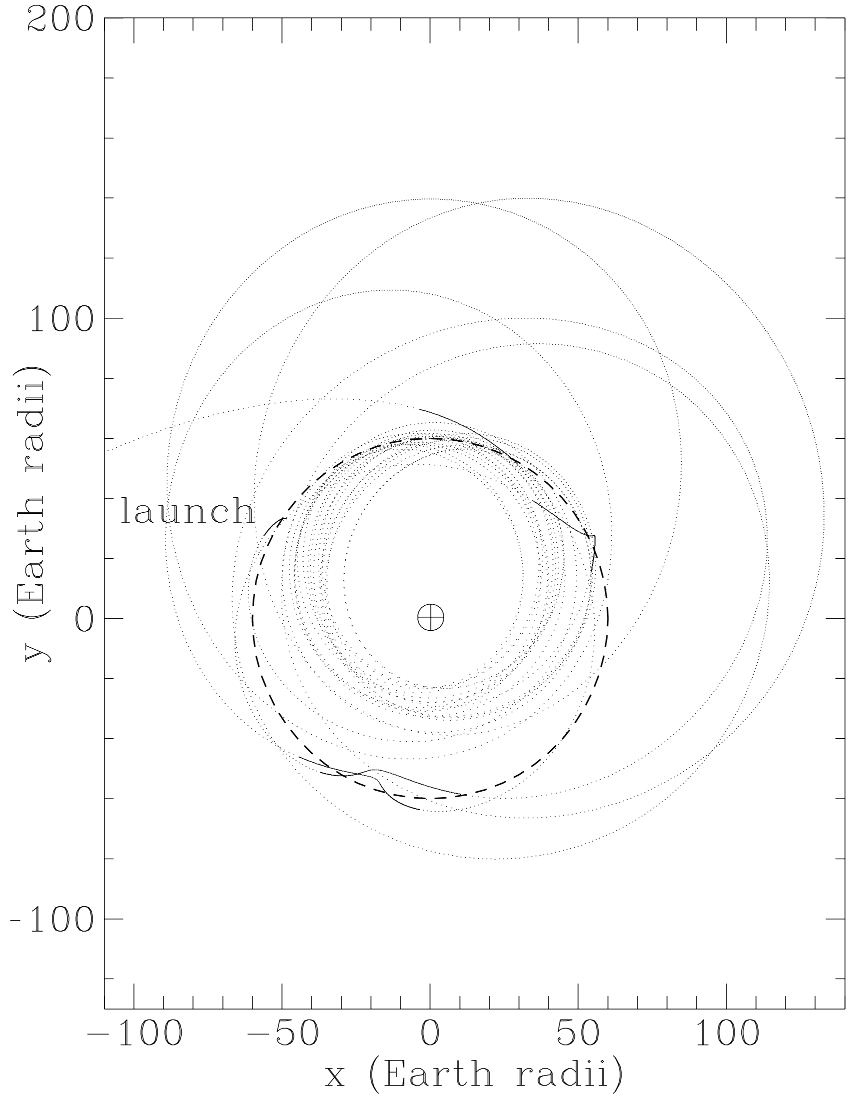

Figure 3.2 The path of a particle escaping from geocentric orbit is shown in a non-rotating geocentric frame, projected onto the ecliptic plane. The particle was launched from the lunar surface at 2.4 km/s. Points are plotted every 3.3 hours unless the particle was within 1 Hill sphere of the Moon (about 9 $R_\oplus$), in which case points are plotted every 0.3 hours (and appear as a solid curve). The dashed circle is at the mean lunar orbital radius (60 $R_\oplus$). The particle is launched from the region just to the right of the word 'launch', outbound on the thick line (due to the Moon's proximity). The multiple close encounters with the Moon before a gravity assist produces escape are typical for particles launched at 2.4 km/s. The particle escapes to heliocentric orbit to the left of the figure after a close encounter with the Moon that provides it with geocentric escape speed. (The Earth's size is not to scale.)

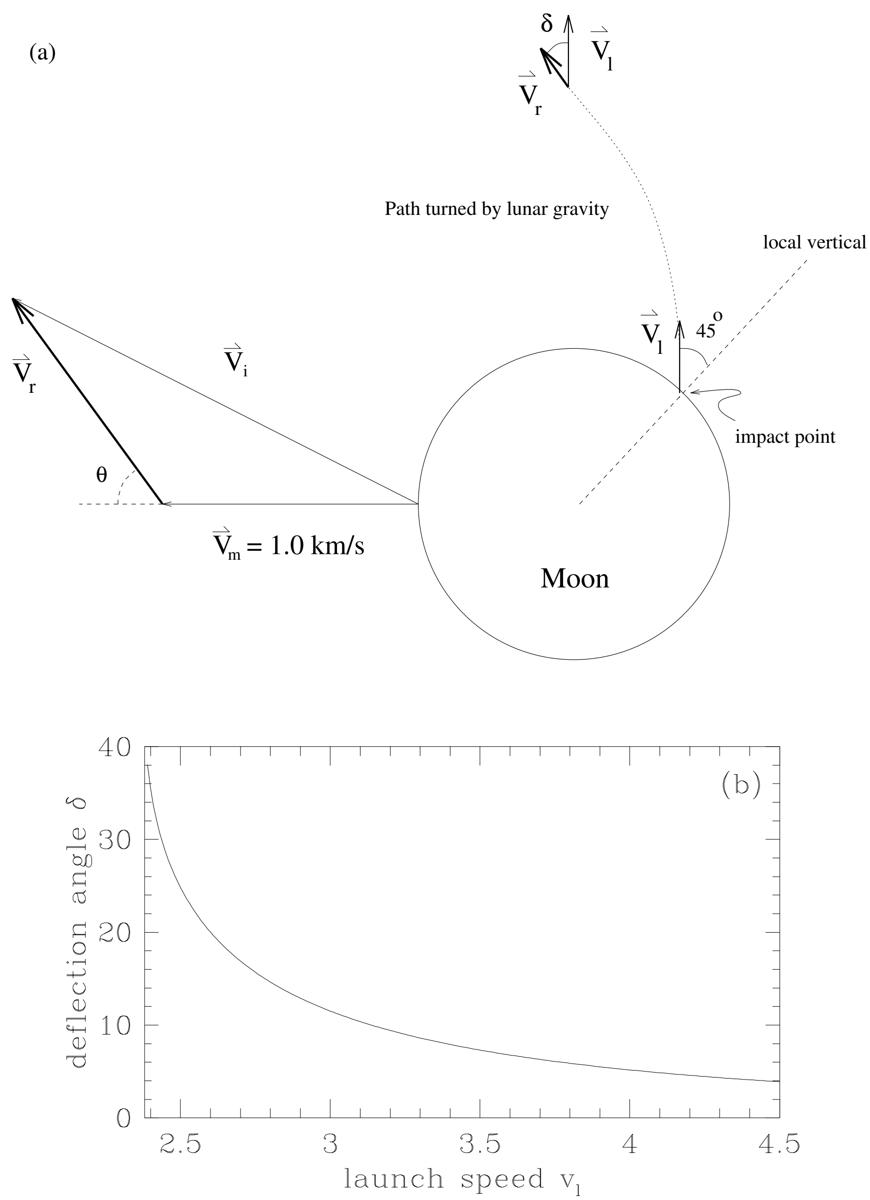

Figure 3.3 (a) A schematic diagram defining various angles for a particle launched from the Moon's surface. Ejecta are thrown at speed v_l and an angle of 45^o to the local vertical off the lunar surface. Due to lunar gravity, the particles are slowed, and their final residual velocity $\vec{\boldsymbol{v}}_{\boldsymbol{r}}$ (measured relative to the Moon) is turned through an angle δ. The initial *geocentric* velocity $\vec{\boldsymbol{v}}_{\boldsymbol{i}}$ is the vector sum of $\vec{\boldsymbol{v}}_{\boldsymbol{r}}$ and $\vec{\boldsymbol{v}}_{\boldsymbol{m}}$, the Moon's orbital velocity. The angle θ between $\vec{\boldsymbol{v}}_{\boldsymbol{m}}$ and $\vec{\boldsymbol{v}}_{\boldsymbol{r}}$ is called the escape angle. Note that *i*) the velocity vectors are not drawn to scale, *ii*) $\vec{\boldsymbol{v}}_{\boldsymbol{r}}$ and $\vec{\boldsymbol{v}}_{\boldsymbol{l}}$ are shown twice on the diagram, *iii*) the figure is for a degenerate planar case, and *iv*) the figure geometry is similar to the launch of the particle of Fig. 3.2. (b) The angle δ, given by (3.1), through which particles departing the Moon are deflected from their launch direction, as a function of launch speed v_l.

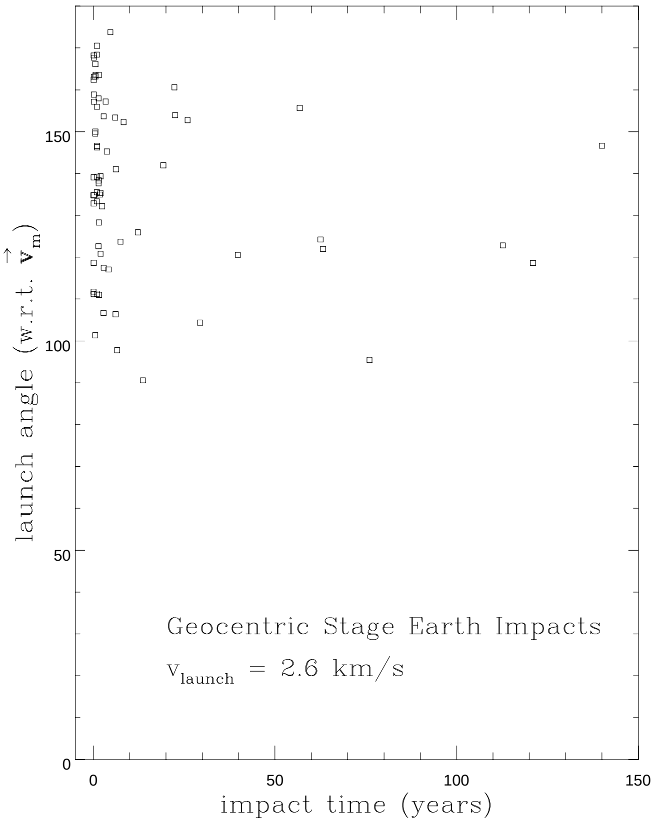

Figure 3.4 The angle between the ejection vector and $\vec{v}_m$ for particles that eventually impact the Earth in a $v_l = 2.6$ km/s geocentric stage simulation. The time until Earth impact is plotted on the abscissa. Particles with angles $< 90^o$ do not impact the Earth since they exceed geocentric escape velocity once free of the lunar gravitational field, and thus escape immediately to heliocentric orbit.

geocentric speeds (which lead to the highest geocentric eccentricities) originate from points $(45 + \delta)^o$ away from the lunar trailing point.

With this as background, let us return to Table 3.2. According to Eq. (3.2), particles with $v_l = 2.6$ km/s escape the lunar field with $v_r = 1.0$ km/s and thus their residual speed equals the lunar orbital speed. If this residual component is vectorially opposite to the lunar orbital velocity ($\theta = 180^o$), the particle will find itself at rest with respect to the Earth after clearing the Moon's gravitational field; thus it will fall directly into the Earth. Particles of this launch speed whose residual components are only roughly anti-parallel to the Moon's velocity will acquire small geocentric velocities; thus they will have prograde geocentric orbits of high eccentricity and, since $v_i < 1$ km/s, will have semimajor axes less than the lunar orbital radius. Subsequent lunar perturbations will push many such particles towards $e \simeq 1$ causing them to impact the Earth. Since their semimajor axes are smaller than the lunar orbit, the Moon's perturbations will have to add

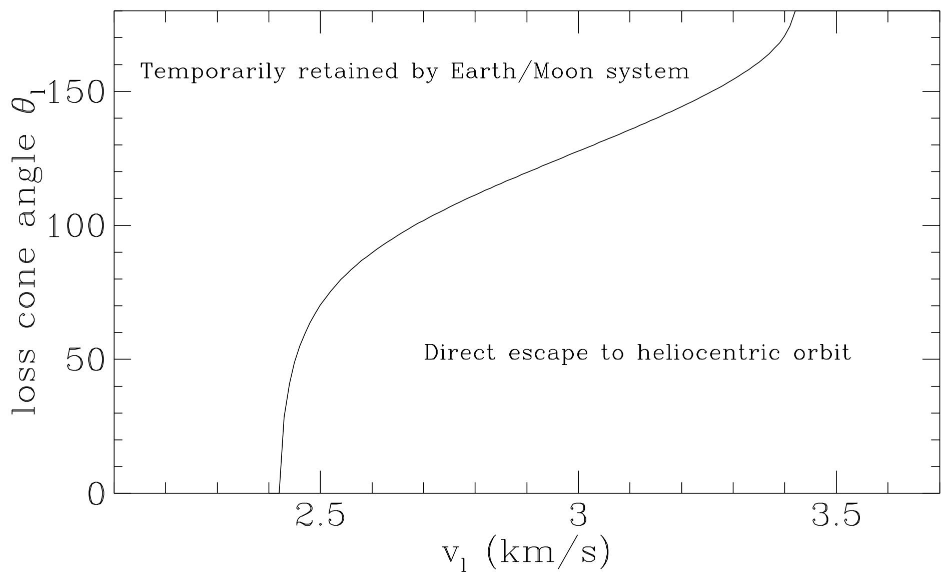

Figure 3.5 The opening angle θ_l of the geocentric loss cone to immediate heliocentric orbit is shown as a function of the launch speed. Particles that have escape angles (after deflection) $\theta < \theta_l$ immediately escape geocentric orbit unless they impact the Earth before reaching their first perigee. The loss cone axis is along the direction of $\vec{\boldsymbol{v}}_{\boldsymbol{m}}$, pointing forward from the Moon's leading point.

constructively to boost these particles finally free from Earth orbit. These two facts explain the increase in Earth impacts at this speed seen in Table 3.2. At the other extreme, $v_l = 2.6$ km/s particles with escape angles less than 90^o have $|\vec{\boldsymbol{v}}_{\boldsymbol{i}}|$ greater than the local geocentric escape speed (of $\sqrt{2}v_{\rm orb} \simeq 1.4$ km/s at the distance of the lunar orbit), and thus exit immediately from geocentric orbit. Figure 3.4 shows clear evidence for this: the Earth is impacted by no particles with an ejection vector within about 90^o of the lunar velocity vector (at launch).

We generalize the above discussion to introduce the concept of a 'loss cone', which is the totality of all escape directions (indicated by $\vec{\boldsymbol{v}}_{\boldsymbol{r}}$) that provide immediate access to heliocentric space. As seen in Fig. 3.3a, these escape directions all lie within some angle θ_l of the lunar motion (i.e., $\theta < \theta_l$ within the loss cone). Fig. 3.5 shows how the opening angle of the loss cone (symmetric about $\vec{\boldsymbol{v}}_{\boldsymbol{m}}$) depends on the ejection velocity; we note that at $v_l \simeq 2.6$ km/s, θ_l is 90^o, so that for this case all (post-deflection) particles moving 'forward' after escaping the lunar field are lost.

At ejection velocities above about 2.6 km/s (where direct transfers to the Earth in a single orbit become permitted since $v_r \geq v_m$), three classes of behavior are possible.

1. Immediate escape (if $\theta < \theta_l$);
2. Immediate collision with Earth (geocentric eccentricity ~ 1); and
3. Geocentric orbit with subsequent lunar perturbations.

Particles in class 1 can still collide with the Earth if, on their outbound path, their trajectories intercept our planet's surface. That this fate occurs often at these velocities can be stressed by considering that at $v_l = 2.8$ km/s a particle launched with $\vec{\boldsymbol{v}}_{\boldsymbol{r}}$ pointed directly at the Earth has $v_i \simeq 1.7$ km/s and sees a gravitationally enhanced cross-sectional area (corrected to v_∞) of roughly 150 times the Earth's geometric area! Above 2.8 km/s significant numbers of particles in class 3 turn out to have very large eccentricities due to the fact that the most likely escape angle is just outside of the loss cone when the loss cone angle is greater than 90^o (due to the $\sin\theta$ dependence of available area on a unit sphere). This explains why the collision percentage at this velocity remains high. Another point of interest is that above 2.6 km/s all of the particles that do not fall inside the loss cone will be on *retrograde* geocentric orbits.

At even higher launch speeds the 'loss cone' for immediate escape widens until at just above 3.4 km/s a particle launched from anywhere on the lunar surface, regardless of the direction of its residual velocity, will leave the lunar field retaining at least the geocentric escape speed. An Earth impact can now only occur if the outgoing path of the particle intercepts the Earth; there will be no subsequent chances. In fact, the simulation for $v_{ej} = 3.5$ km/s recorded no impacts with the Earth or Moon; all particles escaped to heliocentric orbit. For a particle ejected at 3.2 km/s on a trajectory pointing roughly at the Earth, the gravitationally enhanced capture-area is about 20 times the Earth's geometric cross-sectional area. This covers 0.13% of a unit sphere centered on the Moon, so from the 1800 particles launched at this velocity one statistically expects about 2 direct (before first perigee) impacts. In fact 4 were observed.

The claim was made above that there should be no statistical dependence on the 45° angle assumed for the initial launch cone. This was confirmed in a set of experiments presented in Table 3.3, in which the launch velocity was held fixed at 2.4 km/s but the cone angle of the ejected particles was varied. There is no apparent dependence on the angle of the launch cone for the fractions of particles that suffer each fate.

These results on the short-term fate of lunar ejecta, as given in Table 3.2, compare well with those of Gault (1983). My initial conditions differ from Gault's in that I have used a fully three-dimensional model with the Moon in its proper orbit, and I have broken down the statistics by launch speed. Gault's percentages effectively assume a flat spectrum for the numbers of ejected objects as a function of launch speed; when weighted in a similar way, the results agree. In addition, all my geocentric simulations had maximum time limits of 300 years (rather than Gault's 30 years). Gault found that 2 of his 768 particles remained in geocentric orbit after 30 years, while I have no objects (out of more than 8000) that survived as long as 300 years. Escape from the Earth's Hill sphere typically occurs within two months for high-velocity particles inside the loss cone, and within a few years for low-velocity ejecta that require many lunar scatterings to escape. Particles

Table 3.3 For each geocentric-stage simulation (in which all particles are launched from the Moon at 2.4 km/s), the table lists the percentage Esc of particles that escape to heliocentric space and the percentages that impact the Earth ($\oplus$) and Moon (M). The cone angle is the angle with respect to the local vertical of the initial velocity vectors. The 45° simulations are reproduced from Table 3.2

Dependence on cone angle			
Angle	Esc(%)	% $\oplus$	% M
10°	90.5	3.1	6.4
25°	93.0	2.8	4.2
45°	88.1	3.3	8.6
45°	91.7	3.9	4.4
45°	90.0	3.3	6.7
45°	91.1	2.2	6.7
45°	90.5	3.1	6.4
60°	91.7	2.2	6.1
75°	91.6	1.7	6.7
89°	90.7	3.3	5.8

impacting the Earth or Moon usually take several years before doing so, with re-impacts into the lunar surface occurring somewhat sooner. The time distribution of geocentric impacts onto the Earth is shown for one simulation in Fig. 3.4. Note that the lunar meteorites with only upper bounds on their 4π CREs (Table 2.1) could be objects that were delivered to the Earth during their geocentric phase.

3.2.2 Heliocentric Phase

Once the particles move onto a heliocentric orbit, the previous numerical model will be insufficient to describe accurately the continuing orbital evolution of the particles. Experiments show that modelling the system as an Earth–Sun–fragment restricted three-body problem totally fails to capture important facets of the problem. As the Earth's orbit itself illustrates, on a time scale of 10^5 years the influence of the other planets cannot be neglected. To the lowest approximation, the Sun, Earth, and Venus form a three-body subsystem; the planets exchange angular momentum on a time scale of 10^5 years. Jupiter then modulates this interchange on the slightly longer time scale of a few hundred thousand years. I have thus used a regularized, mixed-variable symplectic (RMVS) code in order to perform a full N-body integration of the motion of the test particles. The algorithm is discussed in Appendix B.

The long-term model for the heliocentric simulations includes all planets from Mercury out to Saturn, with the Earth-Moon system in this stage considered as

Table 3.4 Planetary heliocentric ecliptic initial conditions used in the heliocentric stage simulations (note that the Earth-Moon barycenter is integrated). Masses are in $4\pi^2$solar masses and lengths in AU, so that the unit of time is the mean solar year and $G = 1$. The solar radius given is the inner boundary used by the simulations.

Heliocentric Initial Conditions

Object	Mass	Radius
x	y	z
v_x	v_y	v_z
Sun	39.478417604357354	(0.01)
0	0	0
0	0	0
Mercury	$6.5539573684104773\times10^{-6}$	$1.5635249278985897\times10^{-5}$
0.27017937502239237	-0.32228686492574826	-0.051128121581458611
5.8318090354768924	7.0975268449586078	0.044360942040638282
Venus	$9.6636715601426955\times10^{-5}$	$4.0455121263968631\times10^{-5}$
-0.49162157533769937	-0.53077934414038334	0.021133635065132573
5.3678514269101589	-5.0550501344200581	-0.37886320104278040
Earth-Moon	$1.2003167407831363\times10^{-4}$	$4.2634296665828146\times10^{-5}$
-0.82923885617600000	-0.54695064895900000	0.0000610063730000
3.5614549941450000	-5.2271971541900000	0.0006199730700000
Mars	$1.2740275019074827\times10^{-5}$	$2.2707542454345911\times10^{-5}$
-1.5085575023881349	0.70508397896622987	0.051870243545010893
-1.9717133809842210	-4.1945337139270886	-0.039379874024183254
Jupiter	$3.7693444538248594\times10^{-2}$	$4.7721267465874447\times10^{-4}$
-5.3402409482531853	-1.0991402891868280	0.12414342224252320
0.52021430151605930	-2.5741732287263259	-0.00099790164736608
Saturn	$1.1284384051552765\times10^{-2}$	$4.0107522733610672\times10^{-4}$
7.8893232093398913	-5.8757155350551813	-0.21133975684872742
1.1066909037177797	1.6285514822320565	-0.072412495822685855

a single particle at the Earth-Moon barycenter (Table 3.4). The orbital motion of the Moon may be ignored in the heliocentric phase since the (gravitationally focussed) collision cross-section of the Earth is roughly two orders of magnitude larger; this approximation is supported by Whipple and Shelus (1994), who found that the Moon was unimportant in the dynamical evolution of the near-Earth asteroid Toutatis. Particles are removed from the integration once they (i) collide with a planet, (ii) cross the orbit of Jupiter, or (iii) have their perihelia reduced below a lower limit $q_{min} = 0.01$ AU (about 2 solar radii; these particles have become Sun-grazers, a common fate which will be discussed below). The time step used for the lunar simulations (0.015 years) was sufficient to allow for accurate integrations on 10-Myr time scales provided that the particle semimajor axes remained above 0.3 AU; no particles were observed to violate this condition. Within this model, the dynamical evolution of the particles was followed for ten million years (the largest CRE age of a known lunar meteorite).

I have adopted a purely gravitational model for our simulations of 10^7 years duration. If the lunar meteorites existed as decimeter-sized or larger rocks while in space (Warren 1994), radiation pressure forces are negligible over lifetimes of < 10 Myr (see Burns *et al.*, 1979, Eq. 50); these effects are even less relevant for the short CRE age (< 50 kyr) objects. The lifetimes of $\sim 10^2$ g meteoroids at 1 AU against disruptive collisions are estimated by Grün *et al.* (1985) to be only 10^5 years. However, this would seem to contradict the existence of Asuka-881757/Y793169 with its $\simeq 1$ Myr CRE age, and Yamato 81912/86032 with its $\simeq 10$ Myr CRE age (since both of these meteoroids were likely only a few thousand grams while in space) unless the collisional lifetime rises precipitously for masses greater than 10^2 grams. Since the collisional lifetimes derived by Grün *et al.* are intended to model the destruction of dust and are highly model dependent, I will assume below that collisional effects are negligible for lunar meteoroids over $10^6 - 10^7$ year time scales. It turns out that more than 90% of the meteoroids that will eventually return to the Earth do so well within 1 Myr, so if the collisional lifetimes are in fact $\sim 10^6$ years it will have a negligible effect on the age spectrum of the returning objects (see Secs. 3.4 and 4.3).

The usual proviso of numerical celestial mechanics applies to the long-term heliocentric integrations. The Lyapunov times of these particles are so short (several hundred years, Whipple and Shelus 1994) that one cannot claim that the computed trajectories are accurate for specific particles. The calculations must be viewed as statistical studies of the fates of large numbers of particles. Milani *et al.* (1989) and Levison and Duncan (1994) discuss this point further.

After escape from the Earth's influence in the geocentric simulation, particles were inserted into the RMVS simulation with the same position and velocity relative to the Earth-Moon barycenter as they had at the end of the geocentric simulation. The orbital elements for the $v_l = 2.4$ km/s simulation at the time of escape from the Earth-Moon system are shown in Fig. 3.6. The semimajor axes

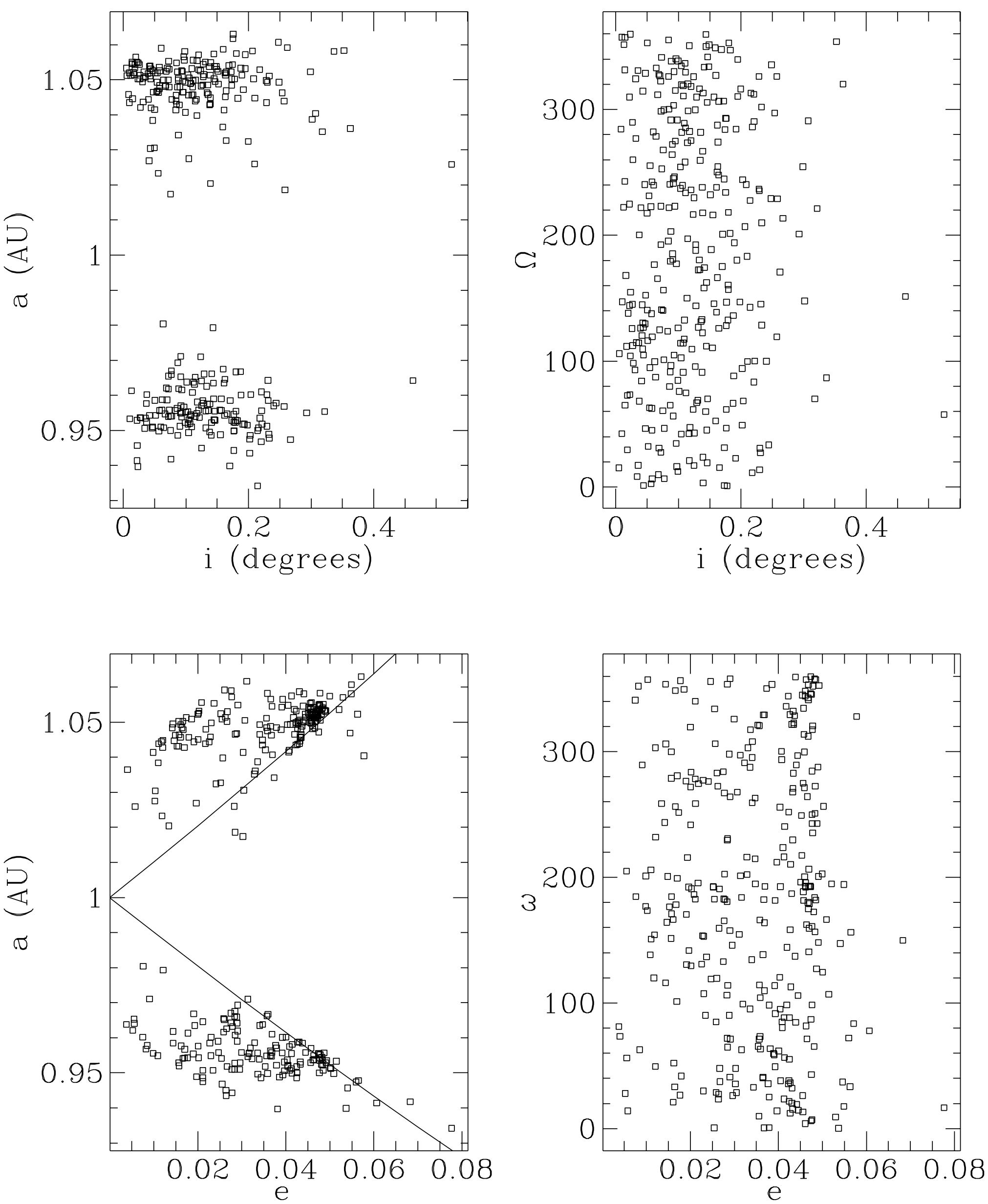

Figure 3.6 The initial orbital elements after escape from the Earth/Moon system for 326 particles originally ejected at 2.4 km/s from the lunar surface. The inclinations (in degrees) are with respect to the ecliptic plane. The two lines in the (a, e) plot show the loci of $q = a(1 - e) = 1$ AU (upper line) and $Q = a(1+e) = 1$ AU (lower line) for reference; particles to the right of these lines cross the Earth's mean orbit. Note that many of the particles are on geometrically non-Earth-crossing orbits (see text).

and eccentricities are those that one would expect for particles that have barely escaped from the Earth-Moon system through the collinear Lagrange points of the Earth-Sun restricted three-body problem. Note the very low inclinations and eccentricities which indicate that many particles escape the Earth/Moon system with only several hundred m/s excess velocity. At these very low relative velocities particles are deflected enough on their outbound paths that they appear to be on geometrically non-crossing orbits in Fig. 3.6, having receded to several Hill sphere radii. However, if time were run backwards, the focussed gravitational cross-section of the Earth is sufficient to bring them to crossing (see, for example, the discussion of Greenberg *et al.* 1991).

The distribution of the particles in Fig. 3.6 is effectively controlled by the requirement that they have almost no velocity relative to the Earth and that they conserve their Jacobi constants on this short time interval. Note the absence of $a = 1$ particles. These are forbidden since an $a \simeq 1$ particle with low eccentricity would be on a horseshoe orbit (Dermott and Murray 1981) and never approach the Earth; clearly a particle launched from the Earth cannot be on such an orbit (by invariance under time reversal). I have studied the $v_l = 2.4$ km/s case in the greatest detail, believing it to be the speed near which most escaping lunar ejecta is launched (as discussed earlier). Given the re-collision rates discussed below, this case is even more important to study since it contributes the largest fraction of the returned meteorites that escape to heliocentric space. The initial conditions for the higher launch speed simulations look similar to Fig. 3.6, but the particles extend to higher eccentricities and inclinations, as well as having a few $a = 1$ particles (which all have high eccentricity).

The particles now proceed to be scattered by the Earth's gravitational field at each conjunction. Some collisions occur, but most objects receive a relative velocity change due to a gravity assist. The a, e evolution of the particle swarm for the 2.4 km/s simulation is shown in snapshots at $10^3, 10^4, 10^5$, and 10^6 years in Fig. 3.7. The general trend is for objects to increase their eccentricities and to walk along the web of lines which maintain either the particle's aphelion or perihelion at one of the terrestrial planets, because on short time scales the local Tisserand invariant T:

$$T = \frac{1}{a'} + 2\sqrt{a'(1-e^2)}\cos i, \tag{3.3}$$

is conserved (Danby 1988); here a' is the ratio of the particle's semimajor axis to that of the scattering planet, and i is their mutual inclination. Note that the lines of $T = 3$ corresponding to small Earth-encounter velocity are not quite the same as $q = 1$ or $Q = 1$ (cf. Greenberg and Nolan 1993). The mean inclination also rises until the particles are roughly uniformly distributed up to 30 degrees (the inclinations at 10^4 years are shown later in Fig. 3.12). After 10^4 years three particles have had close encounters with Venus (they can be easily identified in Fig. 3.7), and after 10^5 years a few have had close approaches with Mars. The

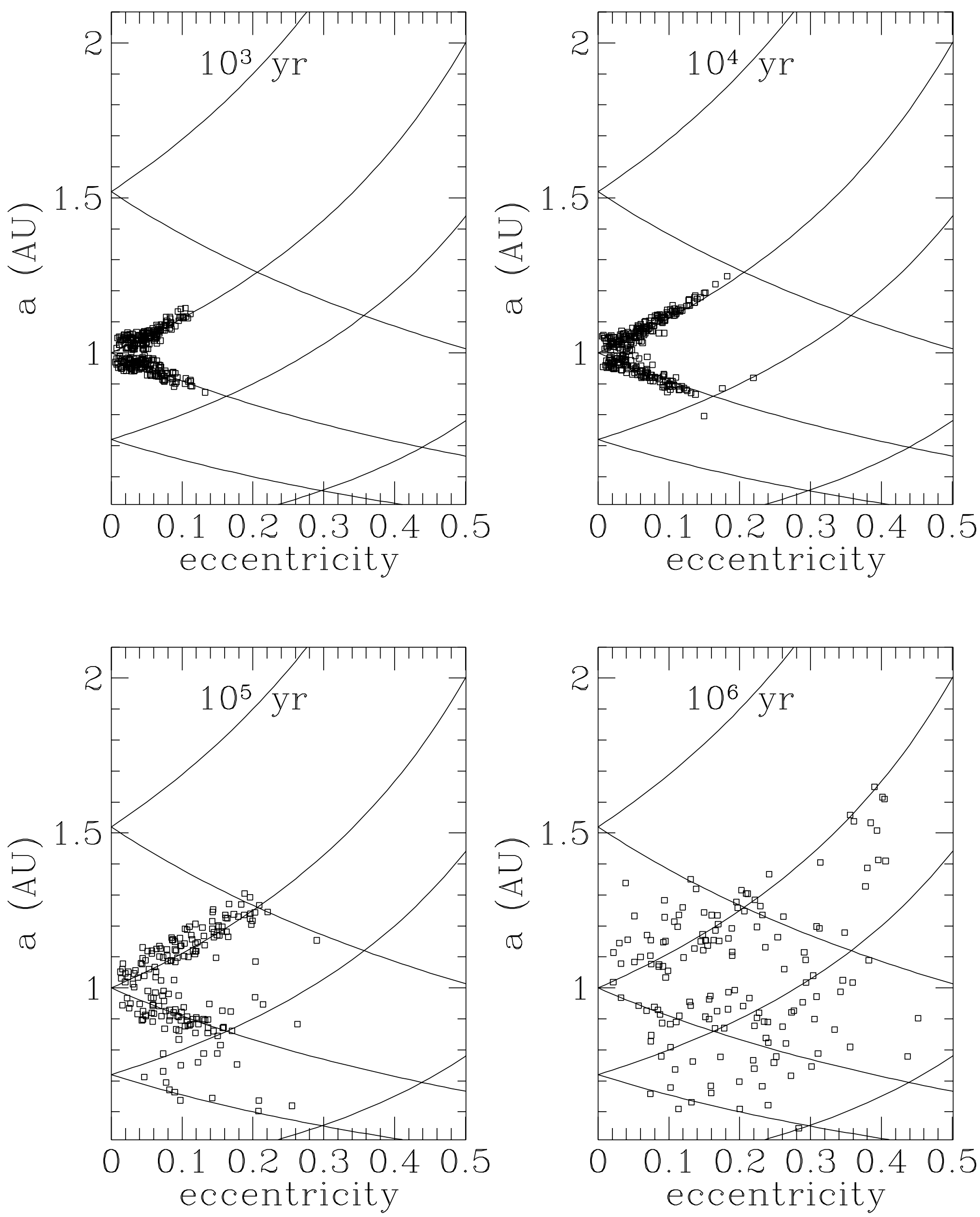

Figure 3.7 Semimajor axes and eccentricities for the surviving particles (from the $v_l = 2.4$ km/s simulation) after 10^3, 10^4, 10^5, and 10^6 years. The lines show perihelia/aphelia at Mercury, Venus, Earth, and Mars; for example, the upper branch of particles in the upper left plot all have perihelia at 1 AU. Particles tend to diffuse along this web of lines due to conservation of the Tisserand parameter with the dominant perturber. This is disrupted by secular perturbations and close encounters with multiple planets.

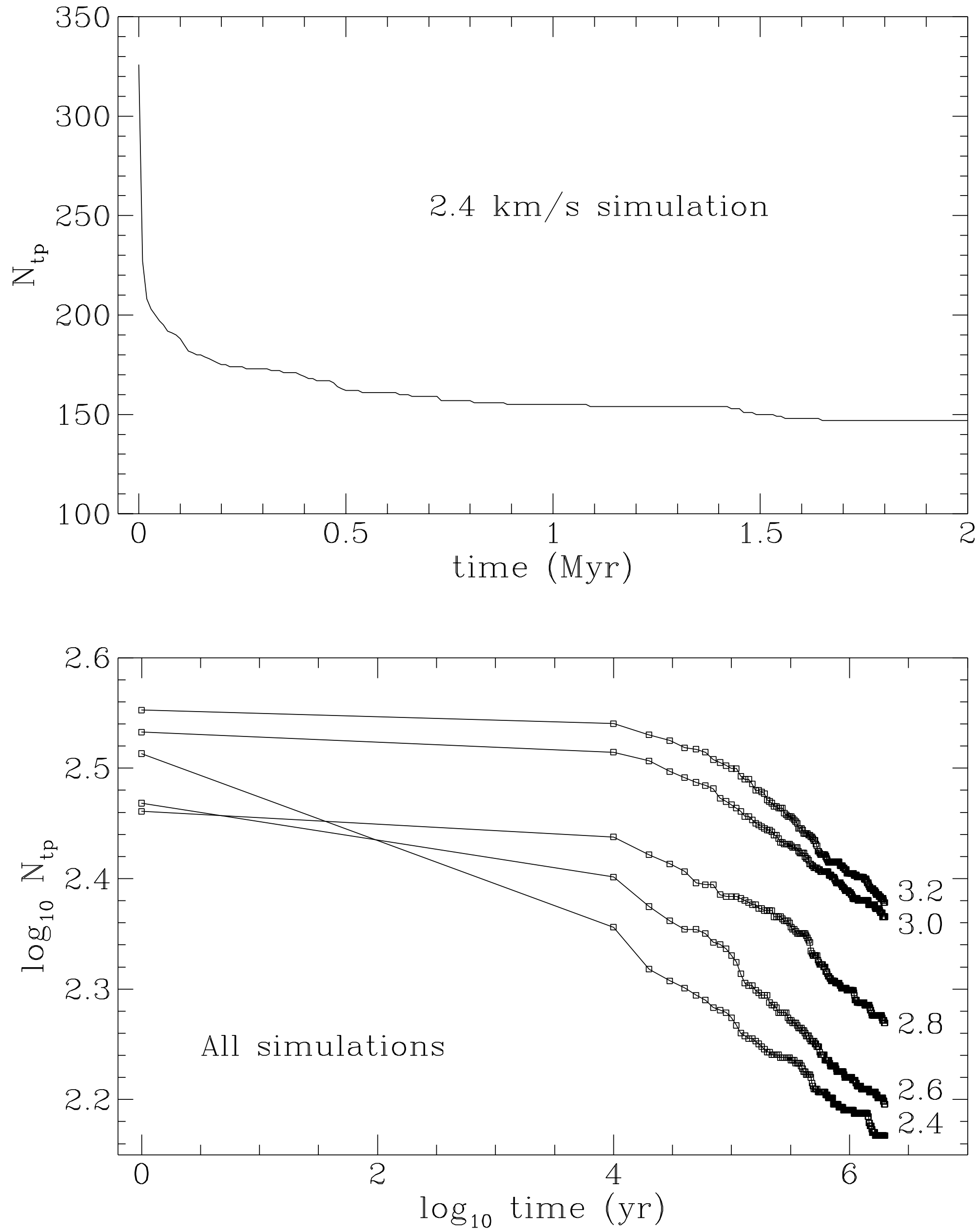

Figure 3.8 The number of particles remaining in a simulation is plotted as a function of time, on a linear plot for the 2.4 km/s simulation (upper panel) and on a log-log plot for all the simulations (lower panel). Loss mechanisms are summarized in Table 3.5. and are not confined to re-collision with the Earth. Note the extremely large loss rate (all from Earth collisions) in the initial stages. The labels in the bottom panel indicate the initial launch speed of the particles. Note that the log-log plot shows that all the simulations eventually follow a common logarithmic fall-off, indicating a similar loss mechanism.

first collision with a planet besides the Earth is, as one would expect, with Venus at 73,700 years after launch. The number of particles remaining as a function of time for the simulations is shown in Fig. 3.8. Note the *extremely* high collision rate initially; more than a third of all the particles that started the 2.4 km/s simulation re-impact the Earth within 50 kyr. The relative loss rate for all the other ejection velocities is also highest in the first 50 kyr. I show below that this is in agreement with the available ages of the lunar meteorites. After the initial burst of collisions, Fig. 3.8 shows that all of the simulations level off to a similar loss rate, which decreases roughly as $1/t$, and seems to be a common result in simulations of swarms of test particles affected by nearby planets (Holman and Wisdom 1993).

The extremely steep initial accretion rate is due to the fact that the relative encounter velocities v_∞ (that is, uncorrected for the acceleration caused by the Earth as the particles fall into its gravity well) are small since they just barely leaked out of geocentric orbit due to a close lunar encounter. The Earth's gravitational cross-section for accretion, the area at ∞ through which passing particles will impact the body, is:

$$\pi b^2 = \pi R^2[1 + (v_{\rm esc}/v_\infty)^2] \tag{3.4}$$

where the planet has radius R and escape speed $v_{\rm esc}$, and b can be interpreted as the impact parameter below which accretion will occur. The Earth's escape velocity of 11.2 km/s dwarfs the typical initial relative velocity of 0.1–1 km/s, resulting in an accretional cross-section several orders of magnitude larger than the Earth's geometric cross-section. If v_∞ were to stay constant, then the number N of surviving particles should follow $dN/dt \propto -N$ and we would expect an exponential drop in numbers. The leveling off of the loss rate apparent in Fig. 3.8 is due to the fact that the relative velocities of the surviving particles are increasing, as evidenced by the spreading of the orbits in 3.7.

Figure 3.9 shows a set of orbital elements for those particles that survived for 10 Myr. The test particles are distributed somewhat uniformly in semimajor axis between Mercury and Mars, and also fairly uniformly in eccentricity from 0 to 0.5. Many particles now have their aphelia inside the asteroid belt and will be prone to collisional erosion (Bottke *et al.* 1994). In any case the fraction of lunar particles that come back to the Earth after having spent more than 1 Myr in the main belt is small, so this effect is not of great importance. It seems that the inner planets are unable to drive particles to $e > 0.5$ or i=25°, and that secular resonances are required (see below). This is not surprising. Even an atmosphere-skimming close encounter directly over a pole of the Earth cannot provide a vertical component of relative velocity larger than $v_{\rm esc}/\sqrt{2} \simeq 8$ km/s, which produces an inclination of no more than 15°.

Table 3.5 lists the reasons for terminating the 224 particles (out of an original 326) that were removed from the 2.4 km/s simulation, as well as similar statistics

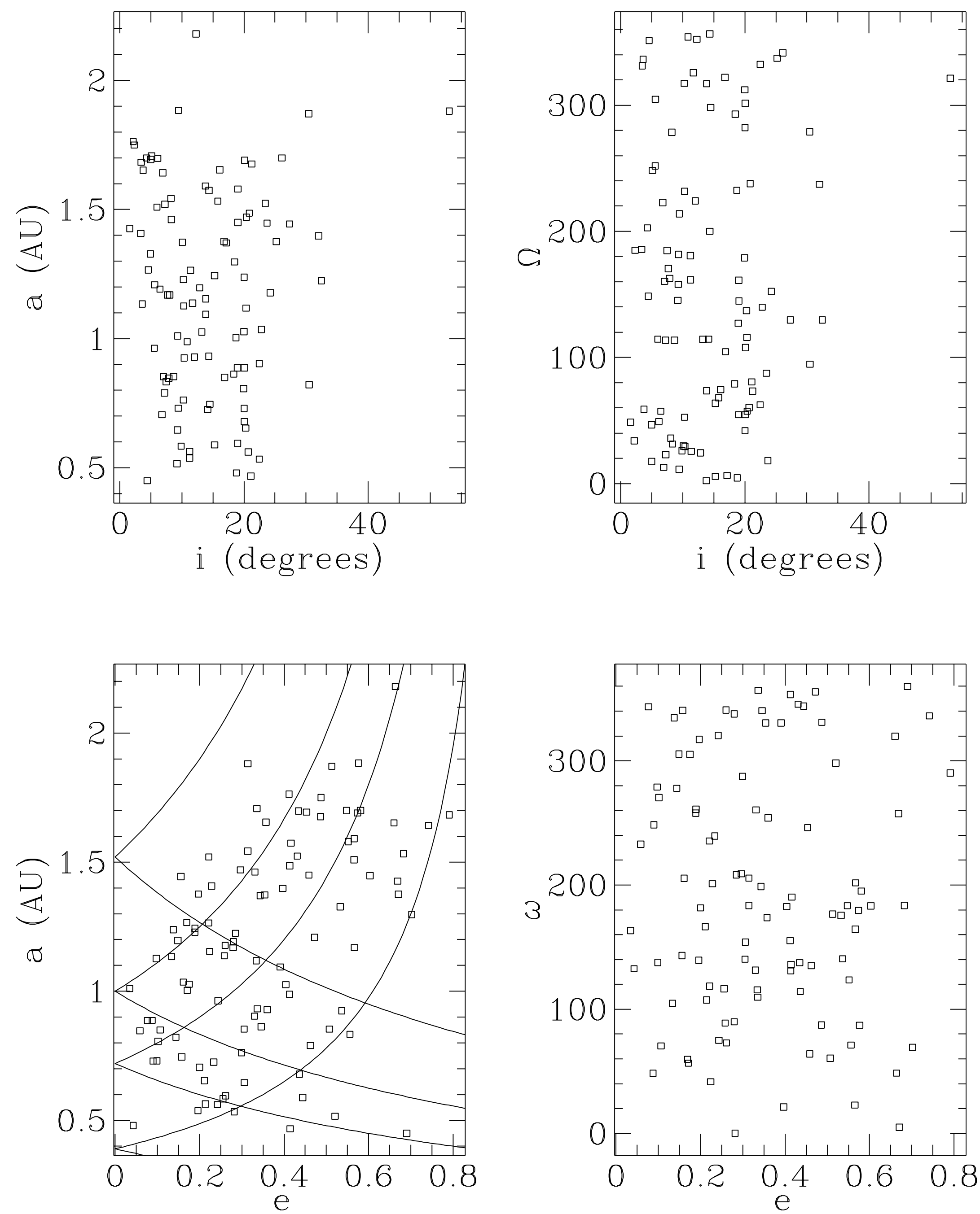

Figure 3.9 Orbital elements for the surviving particles at 10 Myr in the $v_l = 2.4$ km/s simulation. See the text and the captions to Figs. 3.6 and 3.7

Table 3.5 The number of particles removed in each 10-Myr simulation is given for each listed mechanism: collision with a terrestrial planet, or passage into regions of heliocentric space where the simulation would not be accurate. Note the different numbers of starting particles; the remaining particles (out of the 360 launched from the Moon) impacted the Earth or Moon in the geocentric phase.

Heliocentric Stage Removal Statistics					
v_l (km/s):	2.4	2.6	2.8	3.0	3.2
Initial number N_0:	326	294	289	341	357
TERMINATION REASON					
Mercury collision	2	0	0	0	1
Venus collision	23	30	35	41	67
Earth collision	182	142	98	109	96
Mars collision	0	0	1	0	1
$q < 0.01$ AU	14	10	18	18	16
$Q > 6.0$ AU	3	3	3	4	4

for all the other simulations. At the instant of removal we record a particle's position and velocity, as well as those of all the planets, for later processing (to calculate impact velocities and geometries for example). Generically one finds that a large number of collisions occur with the Earth initially and that, after about 500 kyr, impacts with the Earth and Venus occur at roughly equal rates. Two collisions with Mercury were observed in the 2.4 km/s simulation, at t=3.5 Myr and 7.8 Myr after lunar ejection, with impact speeds of 22 and 24 km/s respectively. Only a few collisions with Mars were recorded in all our simulations. The paucity of martian impacts is not surprising since we expect the collision time scale with Mars to be at least several tens of millions of years (from a simple Öpik calculation, see Sec. 3.3). After several Myr the algorithm begins recording the loss of particles inside the q_{min} boundary (they become Sun-grazers). The mechanisms behind this behavior are discussed below.

A typical orbital history is shown in Fig. 3.10. Note the occasional periods of resonance lock, where the semimajor axis is roughly constant and the rate of evolution of the other elements slows down. The lock at $t \simeq 4$ Myr is especially interesting since here the particle has its perihelion well inside the orbit of Venus, yet it is protected by jumping between a series of first-order mean motion resonances with Venus (the 11:12, 12:13, 14:15, and 18:19). The particle's approximately 15° inclination and the Kozai resonance (Michel *et al.* 1995) keep its perihelion at its descending node for several hundred thousand years and thus protects it from close approaches during some of this period. The object shown in the figure entered the Hill spheres of Venus, Earth, and Mars 917, 2454, and 362 times, respectively, during its 10-Myr existence. Most particles that survive

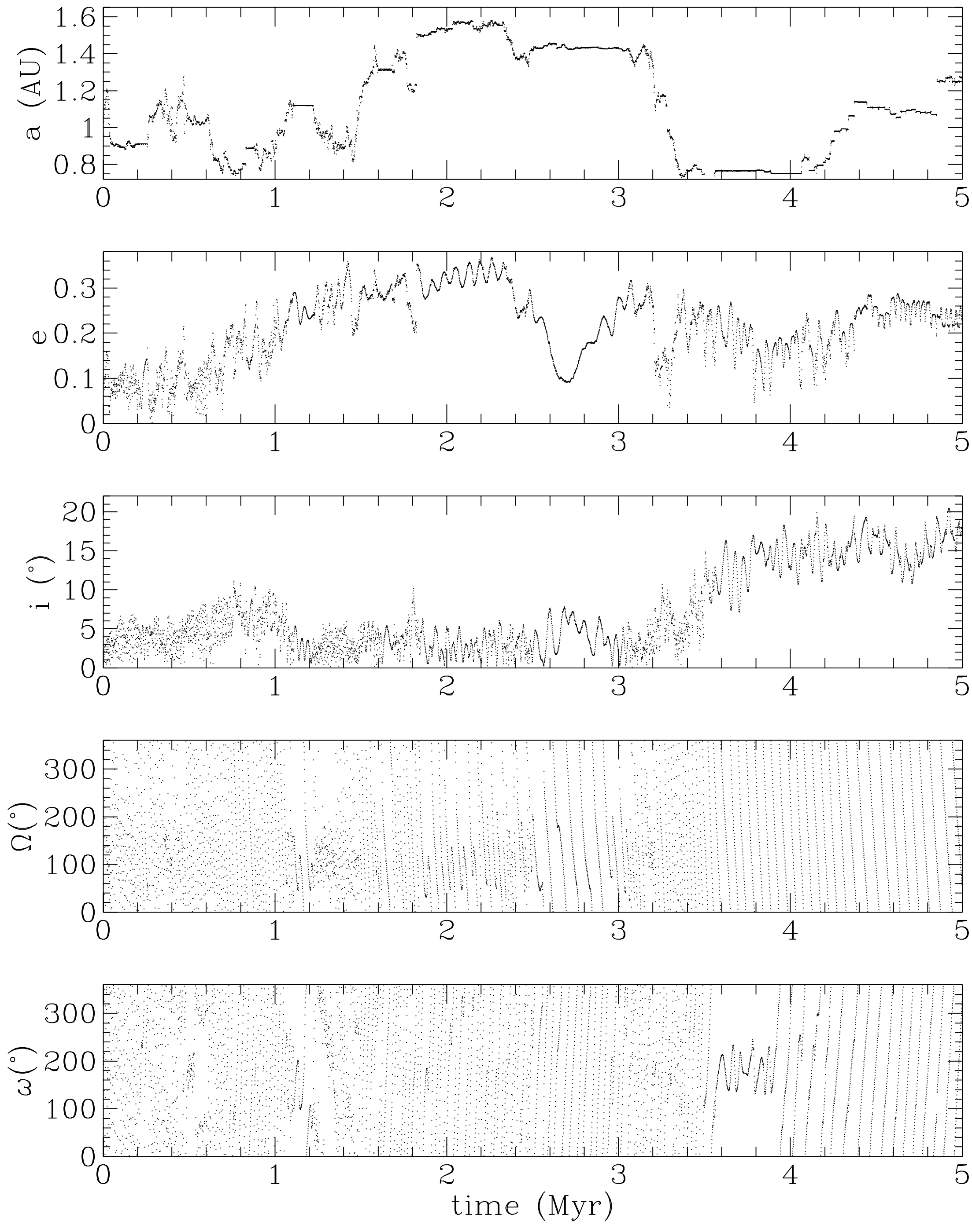

Figure 3.10 Orbital element evolution for the first 5 Myr of a particle launched with $v_l = 2.4$ km/s. See the text for details.

the initial Earth-crossing phase explore much of the inner solar system, being dominated at various times by different terrestrial planets.

An incredibly fascinating array of dynamical behaviors are exhibited by the thousands of particles studied. Most of the particles would belong to the Geographos class for much of their lifetimes, according to the Milani *et al.* (1989) SPACEGUARD classification of Earth-crossing objects. But, for example, the particle shown in Fig. 3.10 is an Eros object from $t \simeq 2 - 3$ Myr. The variety of evolutions is bewildering. Although these dynamical behaviors are not the main point of this study, we shall pause to discuss a few of them.

It was observed that 3-6% of the particles in the lunar simulations became Sun-grazers in the last 8 Myr of the simulations. This fate has been observed in numerical integrations of the orbits of short-period comets (Bailey *et al.* 1992) and near-Earth asteroids (Farinella *et al.* 1994). Almost all of the objects observed to undergo this behavior did so upon having their semimajor axes first modified to $a > 2$ AU, where secular resonances due to the outer planets are located, and subsequently having their eccentricities raised to almost unity. I note, as Farinella *et al.* (1994) do, that this end state is more common than having a particle's aphelion raised to Jupiter-crossing (see Table 3.5). During the final stages of the simulations, Sun-grazing in fact becomes the most common end-state for those particles that are removed. I also note that the particles that end their lives in this way often seem to become influenced by the secular resonances while still deep inside the terrestrial region. Fig. 3.11 displays the orbital history of one of the Sun-grazers. The bottom two panels of this figure show that in the period between 3 and 4 Myr after launch the particle becomes locked in the ν_5 resonance (see Sec. 4.2.1 or Froeschlé and Morbidelli 1994), although this seems to have little effect on its evolution. But near 6 Myr after launch the particle becomes strongly affected by the ν_6 resonance, which proceeds to drive its eccentricity up to nearly unity. However, only a small fraction of the Sun-grazers end their lives while clearly locked in one of these classical resonances. This topic could easily be the subject of considerable further research.

Interesting behavior can also be discovered by mistake. In some of the preliminary simulations (not included here) an error in the transformation to the heliocentric initial conditions caused the escaping particles to be uniformly spread in orbital longitude relative to the Earth at the start of the heliocentric phase. Although easily rectified, this error revealed the existence of Trojan-type horseshoe orbits (although these would NOT come from particles that were launched from the Moon). These orbits exhibited stability for the entire 5-Myr integration, providing independent confirmation of previous hypotheses (Mikkola and Innanen 1992). Whether or not one would expect these stable orbits to be populated in the current solar system is an open question.

Another curiosity is shown in Fig. 3.12 where we exhibit the values of the inclination and longitude of the ascending node for the particles after 10^4 years.

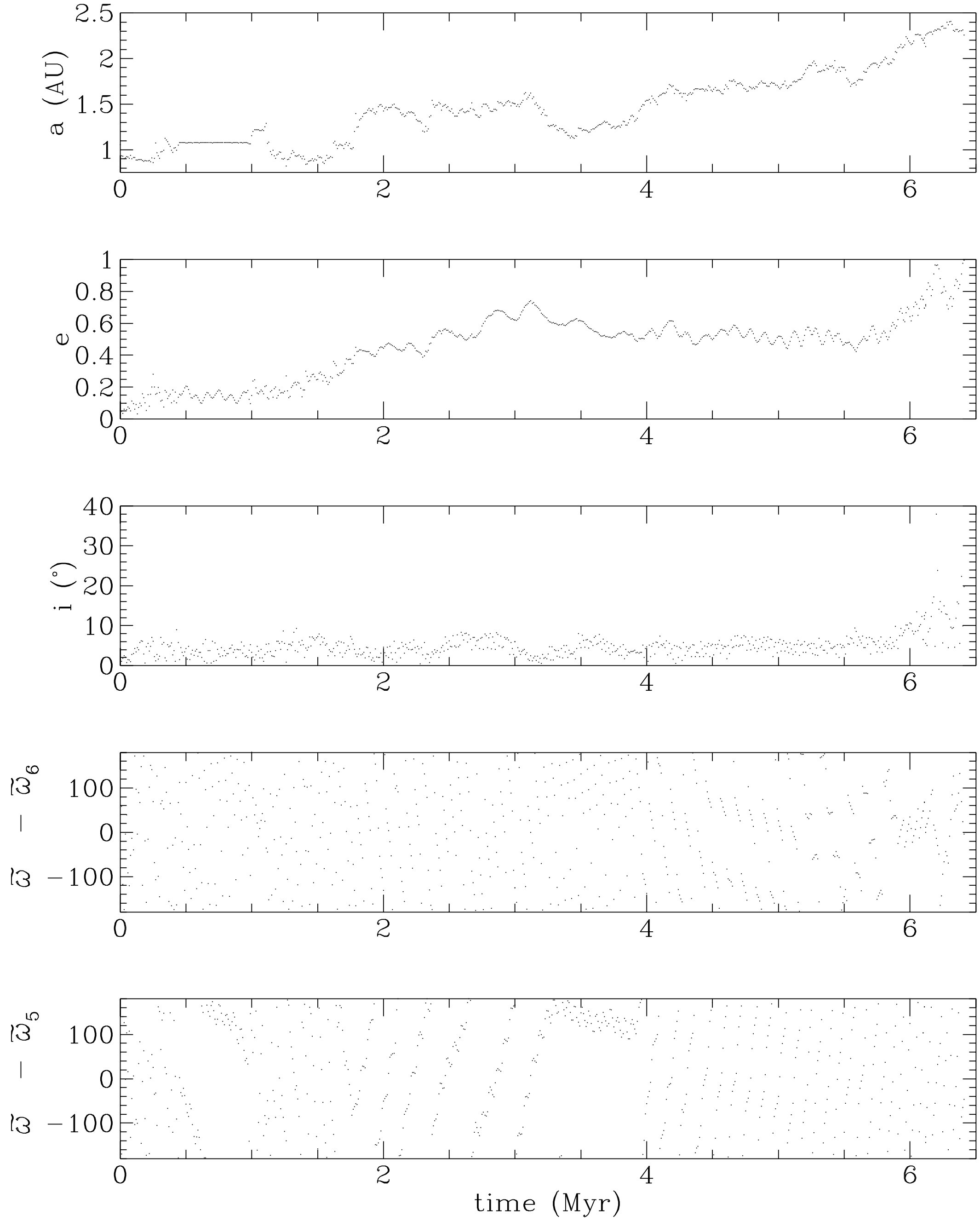

Figure 3.11 The orbital element history of a Sun-grazer. Shown is the a, e, i history for the 6.4 Myr lifetime of a particle from the 2.4 km/s simulation. Also shown are the differences in the longitudes of pericenter of the particle with Jupiter and Saturn. Libration of one of these critical arguments indicates that the particle is locked in the resonance. Observe that the eccentricity is driven to 1 when the ν_6 resonance is entered near $t = 6$ Myr.

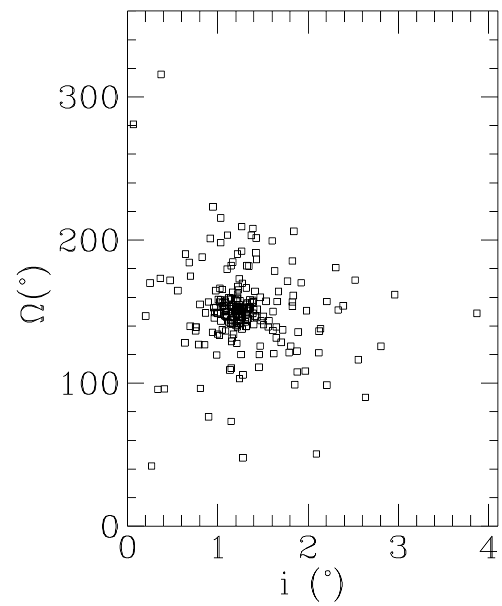

Figure 3.12 The inclination of the test particles in the 2.4 km/s simulation after 10^4 years of evolution. The particles are preferentially confined to have their orbital planes coincident with the Earth.

The initially uniform distribution has now been strongly concentrated towards $\Omega \simeq 150^o, i \simeq 1.2^o$, which are the Earth's values at this epoch. Compare this with Fig. 3.6, in which the initial nodes are randomly distributed. This apparent concentration is a coordinate-system artifact caused by referencing all the inclinations and nodes to the initial ecliptic plane. The test particles have all been precessing around their Laplace planes (see Ward 1981); the latter planes have been following the Earth's slowly moving orbital plane, which is rotating mostly due to the Earth's interaction with Venus. Since the particles all have almost zero free inclination initially, the dominant secular effect will be to maintain this state. This will be disrupted by close encounters which gradually raise the mutual inclinations of the particles with the Earth. Once the mean mutual inclination reaches the Earth's instantaneous inclination (with respect to the reference plane), this correlation disappears. This requires several hundred thousand years, and it can be seen that such a concentration is absent in Fig. 3.9. When the nodes are measured with respect to the Earth's *instantaneous* orbital plane, the distribution is indeed random. This common precession of the nodes with respect to another fixed plane (whether it be the ecliptic plane at t=0 or the invariable plane) is a very important effect since it keeps the mutual inclinations with the Earth low and thus the collision probabilities (as discussed in the next section) high. It would be erroneous to compute collision rates (using an Öpik

Table 3.6 For each launch speed v_l (km/s) N_o particles escaping to heliocentric orbit were followed for 10 Myr (all times are in Myr). The number of particles N_{tp} still in the simulation (allowing for *all* removal mechanisms) at $t = 0.05$, 1, and 10 Myr is then given. The number removed by *Earth collisions* during the geocentric simulation, and the heliocentric simulation in the time intervals 0-50 kyr, 50 kyr–1 Myr, and 1–10 Myr, is shown. The percentages for these cases are given in the last 3 columns, with the geocentric collisions absorbed into the <50 kyr column.

Heliocentric Stage Results											
	N_{tp}				Number of $\oplus$ collisions				% $\oplus$ collisions		
v_l	$N_\circ$	0.05	1.0	10.0	Geo	≤0.05	0.05-1	1-10	≤0.05	.05-1	1-10
2.4	326	197	155	100	13	129	33	20	73	17	10
2.6	294	226	166	109	65	68	51	23	64	25	12
2.8	289	249	199	155	69	49	26	23	71	16	14
3.0	341	307	244	174	18	33	49	13	45	43	12
3.2	357	329	254	171	2	27	53	16	30	54	16

theory for example) assuming that the relative node on the reference plane of the test particles and the Earth was distributed uniformly.

Table 3.6 summarizes all the heliocentric stage simulations, as well as information on the impact distribution (in time) of the objects that strike the Earth. Each simulation started with $N_\circ \sim 300$ test particles (all of which had originally been ejected from the Moon at a common speed) and lasted for 10 Myr. The number of test particles surviving at 50 kyr, 1 Myr, and 10 Myr is shown to give some idea of the loss rate, and includes all the loss mechanisms summarized in Table 3.5. I then present the information on only the Earth collisions, which are relevant for comparisons with the lunar meteorite data. These same data are presented in a more detailed graphical format in Fig. 3.13, and will be discussed further below.

3.3 Comparison with Monte Carlo Methods

An alternate approach to the heliocentric stage of this problem would be to conduct a Monte Carlo simulation of the orbits of the particles. In this method, collision probabilities (Öpik 1976) are used to calculate the frequency of close approaches, at which time collisions or orbital modifications occur after randomly determining the close encounter distance; when implemented numerically this is called an Öpik-Arnold approach. In this way Arnold (1965) and Wetherill (1968) found a steep spectrum of expected collision ages with the Earth, with the vast majority of the collisions occurring in the first Myr (see Arnold's Fig. 2 or Wether-

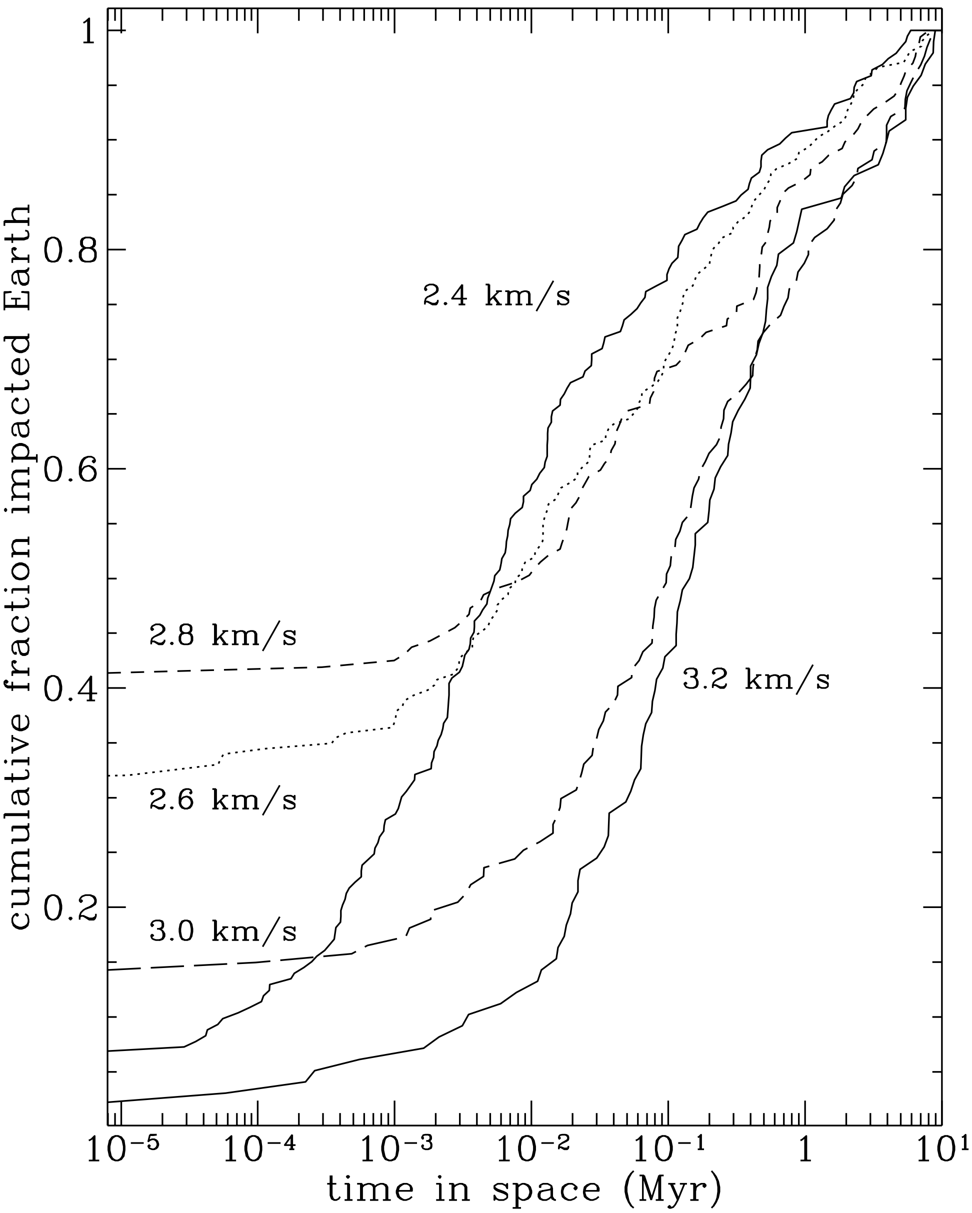

Figure 3.13 This plot presents, as a function of time, the cumulative fraction of simulated meteorites that have arrived on the Earth, to all those that will within 10 Myr. One curve is shown for each lunar launch speed. For example, by 0.1 Myr 40% of the meteorites that will arrive have returned to the Earth for the $v_l = 3.2$ km/s simulation, whereas about 80% of the meteorites delivered in the 2.4 km/s simulation have already arrived by that same time. For the purposes of this figure all geocentric deliveries were deemed have arrived in <10 years; these deliveries are responsible for the non-zero values at t=10^{-5} Myr.

ill's Fig. 7). Until recently, it has not been feasible to carry out direct integrations of particles that are in close-crossing orbits in order to confirm the Monte Carlo results (although Milani *et al.* 1990 conducted a $\sim 10^5$ year comparison for the deep Earth-crossing asteroids). The RMVS code now allows us to do this.

The subject of study here is especially difficult for an Öpik approach since the initial orbits are very Earthlike and thus have tiny relative velocities. This causes degeneracies in the Öpik equations, owing to the many cases of small mutual inclinations, tangent orbits, and partial crossings. A comparison of my results with Monte Carlo simulations (G. Wetherill, private communication, 1994) shows that over a variety of time scales the Öpik approach underestimates the re-collision fraction with the Earth by factors of 3 to 12. The error lessens as the length of the simulation is extended: the more than order of magnitude error in the fraction of returned objects during the first 10^5 years is reduced to a factor of three if one considers 10-Myr time scales. Despite this problem, the overall *relative* distribution of re-collision ages (e.g., the fraction of objects returning within 10^5 years compared to those that return within 10^7 Myr) given by the Monte Carlo approach is roughly correct (to within a factor of a few). This conclusion is also reached by Dones *et al.* (1996a).

The comparatively short recollision times found early in both the Monte Carlo simulations and the direct integration principally result from the low relative velocities of particles with respect to the Earth. As the particles scatter repeatedly off of the Earth's gravitational field, the relative velocities increase and collisions become less likely. Thus, all methods should find a steep drop-off in the collision rate as the Earth's gravitationally enhanced cross section shrinks *and* the number of impactors falls because collisions are occurring. The resulting 'faster than exponential' drop in the impact rate is apparent in Fig. 3.8.

The initially Earth-like orbits of the particles introduce complications for the Öpik-Arnold approach. Furthermore, as noted above, much of the evolution in the simulations is influenced by the presence of resonances. Resonance effects are clearly important, but the manner in which they affect the results is complicated. In fact, the common occurrence of short-term resonance locks is likely one reason why the Öpik collision rates are in error. The Monte-Carlo methods also suffer from an inability to discover interesting dynamical processes like those discussed in the previous section. These issues are further explored by Dones *et al.* (1996b). The Öpik approach provides a good qualitative understanding of the problem nevertheless. In fact, the Monte Carlo calculations were well suited to address the questions posed originally by Arnold and Wetherill (namely, a possible lunar origin for chondrites and the time of fall asymmetry). In summary, I find that the steep collision spectrum found by the method used by Arnold and Wetherill is correct, but a large fraction of the material returns in only 50 kyr, and that the absolute yields are too low by a factor of a few.

3.4 Comparison with Lunar Meteorite Data

I now return to the CRE data on the lunar meteorites (Table 2.1). How do the CREs of the meteorites compare with the simulated collision results, and what can be said about the transfer process from the available samples? Of the eleven objects with reliable ages, seven have CREs of less than 50 kyr, although all but one of these are upper limits. Fig. 3.14 compares the cumulative distributions of the expected CREs from the $v_l = 2.4$ and 3.2 km/s simulations with the available data. The plot includes those particles that impacted the Earth while still in the geocentric stage. Since the collisions occur so quickly in the initial part of the simulation, it is best to examine the distribution binned logarithmically in time. The steep time spectrum is in qualitative agreement with the CRE age data, with a large amount of material returned in less than 0.1 Myr; in fact, for the 2.4 km/s simulation more than half of the returning material arrives in less than 10 kyr.

The prevalence of upper limits on the 4π CRE ages is due to the difficulty of measuring the presence of isotopes having such short half-lives and small abundances in the meteorite. Thus, Fig. 3.14 does not very well discriminate amongst launch velocities, nor is it probably a very good representation of the actual spectrum, since the meteorites could very well have 4π ages orders of magnitude smaller than their upper limits. To obtain a fairer comparison I have re-plotted the data using the thermoluminescence ages from Table 2.1 for the lunar meteorites that have only upper bounds on their CRE ages (Fig. 3.15; *cf.* Sec. 6.2.5). For objects that have only upper bounds on their CRE and thermoluminescence ages, I have assumed a 100-year transit time (which could be in either the geocentric or heliocentric stages). Fig. 3.15 shows that, given the small sample of actual lunar meteorites, the 2.4 km/s model provides a reasonable match to the data. The 3.2 km/s simulation delivers almost all its meteorites in the period after 50 kyr from launch, in disagreement with the data. Unfortunately, the 11-object sample size means that the cumulative distribution may be significantly altered by the addition of another data point. Although the spectrum derived from the data in Fig. 3.15 is somewhat ad hoc, it is almost certainly a more accurate representation of what the real delivery spectrum looks like than Fig. 3.14.

3.4.1 The lunar velocity spectrum

Because the delivery spectrum (in time) changes as the launch speed varies, we are able to rule out a large preponderance of higher launch speeds since they have a much smaller fraction of quick deliveries (due to having much higher relative velocities to the Earth after the initial escape to heliocentric orbit). Referring back to Fig. 3.13, we see that if $v_l \leq 2.8$ km/s then approximately half of the meteorites should have transit times of less than a few thousand years (with the interesting difference that for $v_l \approx 2.6 - 2.8$ km/s most of these rapid returns

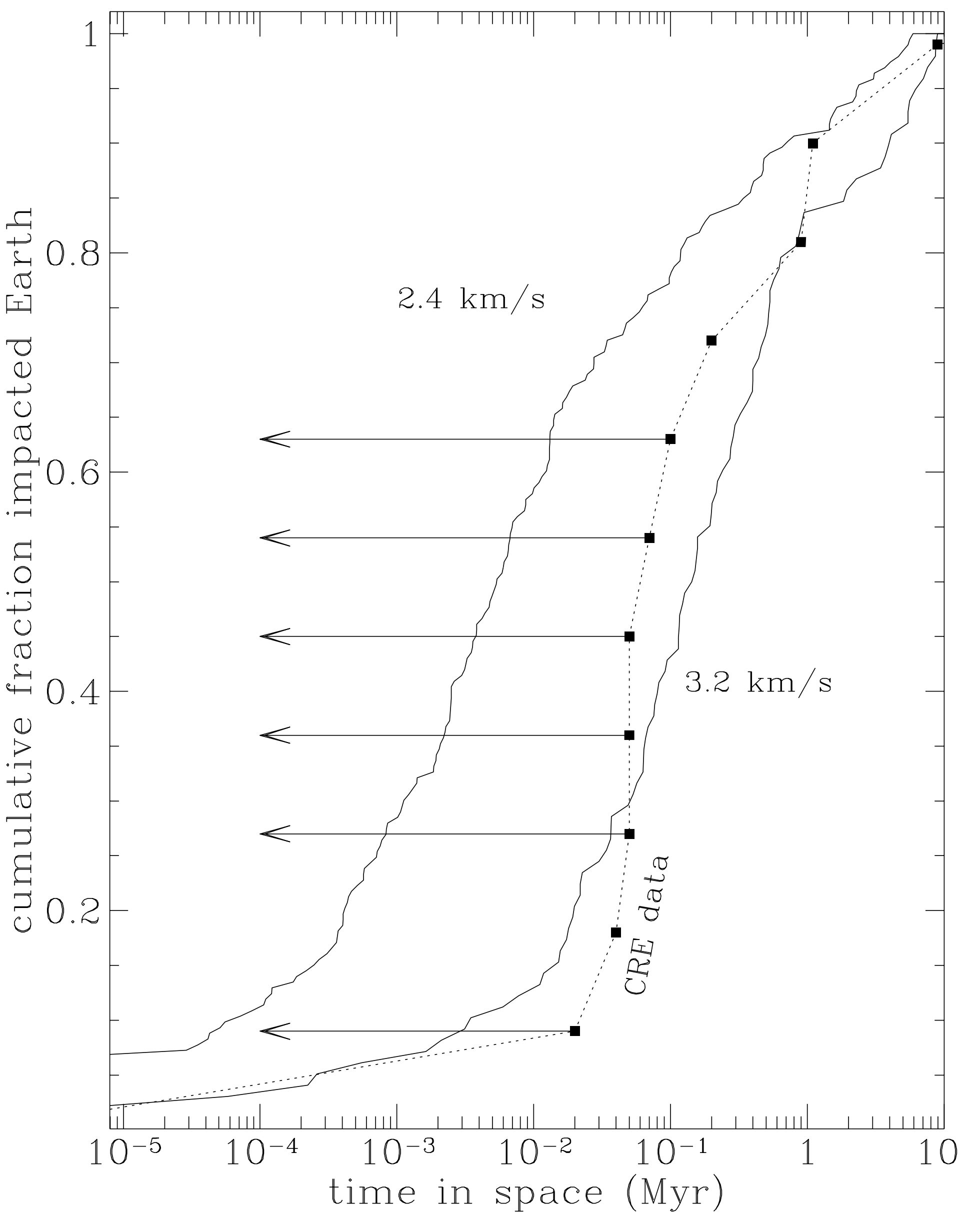

Figure 3.14 The time spectrum of the CRE age data for the lunar meteorites is compared with two of the simulations. See the caption to Fig. 3.13 and the text. The arrows indicate that the data point is only an upper limit of the 4π age of the meteorite.

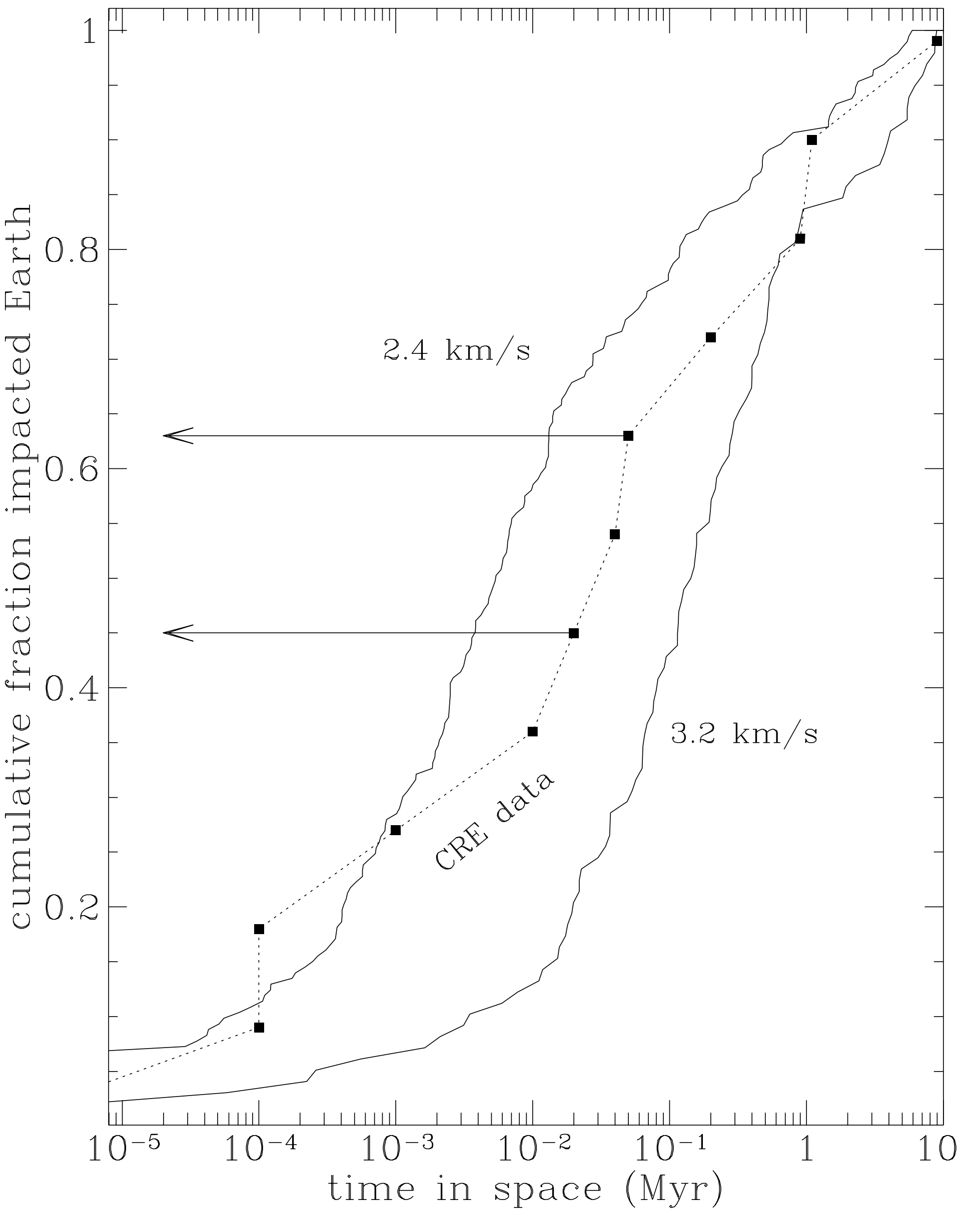

Figure 3.15 Cumulative spectrum, modified TL data and assumed geocentric impacts, as explained in the text.

actually take place in the geocentric stage). Because of the prevalence of upper limits in the transit time data, we cannot say for certain if this is true of the meteorites. However, above $v_l = 3$ km/s, one must wait 0.1 Myr for half of the meteorites to arrive. Therefore we can conclude that most of lunar meteorites must be launched with $v_l < 3$ km/s, for if this were not the case very few would have CRE ages < 0.1 Myr. Since the ejecta velocity distribution is likely some form of a power law, the strongest statement that can be made is that not all of the lunar meteorites were launched with speeds > 2.6 km/s. This can be quantified in the following way. If the number of meteoroids ejected at velocity v ($v > v_{\rm esc}$) obeys

$$N(v)dv \propto v^{-p} dv \; , \tag{3.5}$$

then the fraction of particles (of those that escape) that leave with velocity $v > v_*$ is

$$f = \frac{N(v > v_*)}{N(v > v_{\rm esc})} = \left(\frac{v_{\rm esc}}{v_*}\right)^{p-1} . \tag{3.6}$$

The experimental results of Gault *et al.* (1963) imply $p \approx 4.5$ (Wetherill 1984), in which case Eq. 3.6 implies that $\approx$ half of the ejecta should leave at faster than 3 km/s. This is consistent with the data since then, weighting the contributions of the various launch speeds given in Fig. 3.13, about 30% of the meteorites should arrive in 6,000 years and 65% in 0.1 Myr, in good agreement with Fig. 3.15. Further discussion of this topic will be postponed until Chpt. 6.

It is again worth nothing that, at launch speeds of $v_l = 2.6$ and 2.8 km/s, a large fraction of transfers with CREs < 50 kyr happen in the geocentric phase (see Table 3.2). Thus, in these cases (see Table 3.6), the deficit of fast heliocentric returns is more than compensated for by the large number of geocentric stage impacts. This makes the velocity spectrum (given roughly by the last three columns of Table 3.6) difficult to distinguish from the 2.4 km/s case if one cannot separate out those lunar meteorites that never left geocentric orbit. If the geocentric stage meteorites could be distinguished from those that escaped to heliocentric space on the basis of their CRE ages, one might be able to rule out $v_l = 2.6 - 2.8$ km/s as a common launch speed, since for these velocities lunar meteorites with CRE ages <300 years should comprise a fair fraction of the objects (about a third). Measuring such short cosmic ray exposure ages is unfortunately very difficult, if not impossible; thus the current upper bounds on many of the 4π CRE ages in Table 2.1 are insufficient to determine whether or not these particular objects escaped to heliocentric space. Measurement of short CRE ages would require a lunar fall to be observed (so that the residence time on the Earth is known to be negligible); it is likely that we must wait awhile for a statistical sample.

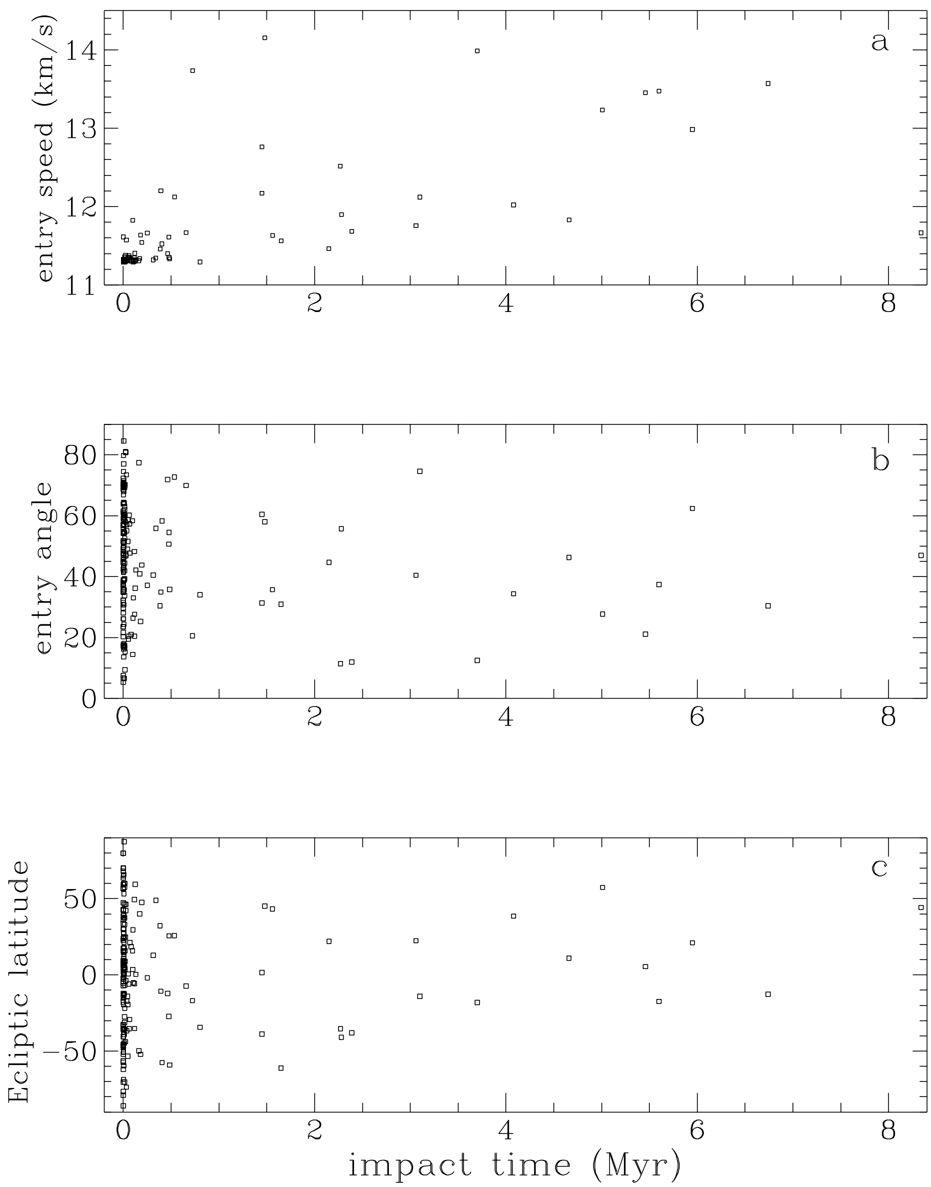

Figure 3.16 Collisional data as a function of time for the heliocentric stage impactors in the 2.4 km/s simulation. (a) Entry speed at the top of the atmosphere. (b) Entry angle (with respect to local vertical). (c) Ecliptic latitude of the impacts on the Earth.

3.4.2 Entry statistics

Fig. 3.16 displays additional information on the collision circumstances of the Earth-impacting particles from the heliocentric stage of the simulation. Figs. 3.16a and b, respectively, give the entry speed and angle (with respect to the local vertical) at the top of the atmosphere at the time of collision. As one would expect, because the orbits of the particles are very Earthlike early in the simulation, the entry velocities then are just barely above the Earth's escape velocity of 11.2 km/s. (Of course, the entry velocities of *all* the impacting particles during the geocentric phase are also just above the escape speed since such particles start at the lunar orbit with geocentric velocities small compared to 11.2 km/s). The mean entry velocity for heliocentric stage impacts rises with time as the average eccentricity and inclination (and hence encounter speed) of the particle swarm rise. This will presumably produce a slight bias *against* lunar meteorites with CREs $>$ 1 Myr since they will suffer heavier ablation; perhaps a factor of 2 more mass loss if the entry velocity rises from 12 to 18 km/s (ReVelle 1979). Furthermore these same objects will have been more prone to collisional disruption near their aphelia (Bottke *et al.* 1994). This bias will presumably concentrate the distribution of *recovered* meteorites somewhat more strongly towards younger ages. The entry angles α (Fig. 3.16b) for the returning heliocentric particles follow a $\sin 2\alpha$ distribution as expected (see Shoemaker 1962). In contrast (see Fig. 3.17), the entry angles for the geocentric stage impactors have a small bias to be concentrated towards larger entry angles (i.e., shallower entries). The mechanism that causes this effect is simply that the particles are in geocentric orbits that are perturbed into collision by having their perigees lowered to (most likely) just below the Earth's radius, resulting in an entry closer to tangency. This does not violate the standard $\sin 2\alpha$ result since the geocentric stage impactor-flux does not satisfy the assumption of being isotropic nor is it comprised of hyperbolic orbits coming from infinity. This could result in a slightly higher survival rate, due to less severe ablation, for particles that impact the Earth without having ever reached heliocentric orbit.

To examine the expected distribution of lunar meteorites on the Earth, I plot the *ecliptic* latitudes of the entry points in Fig. 3.16c. I have used the latitude on the Earth with respect to the ecliptic plane since I have not kept track of the Earth's polar precession in the simulation. Thus the latitudes with respect to the Earth's equator may differ by as much as $\pm 23°$. Nevertheless, a χ^2 test shows that the distribution on the Earth is statistically consistent (at the usual 5% level) with uniformity (i.e., there are no favored latitudes). The Earth should be uniformly covered with lunar meteorites, and there is no bias for or against Antarctica on dynamical grounds (cf. Halliday and Griffen 1982, who claim a slight 15% observational bias against polar returns for fireballs). The unbiased distributions of impact latitudes is also true for those particles colliding during the geocentric stage of the simulations.

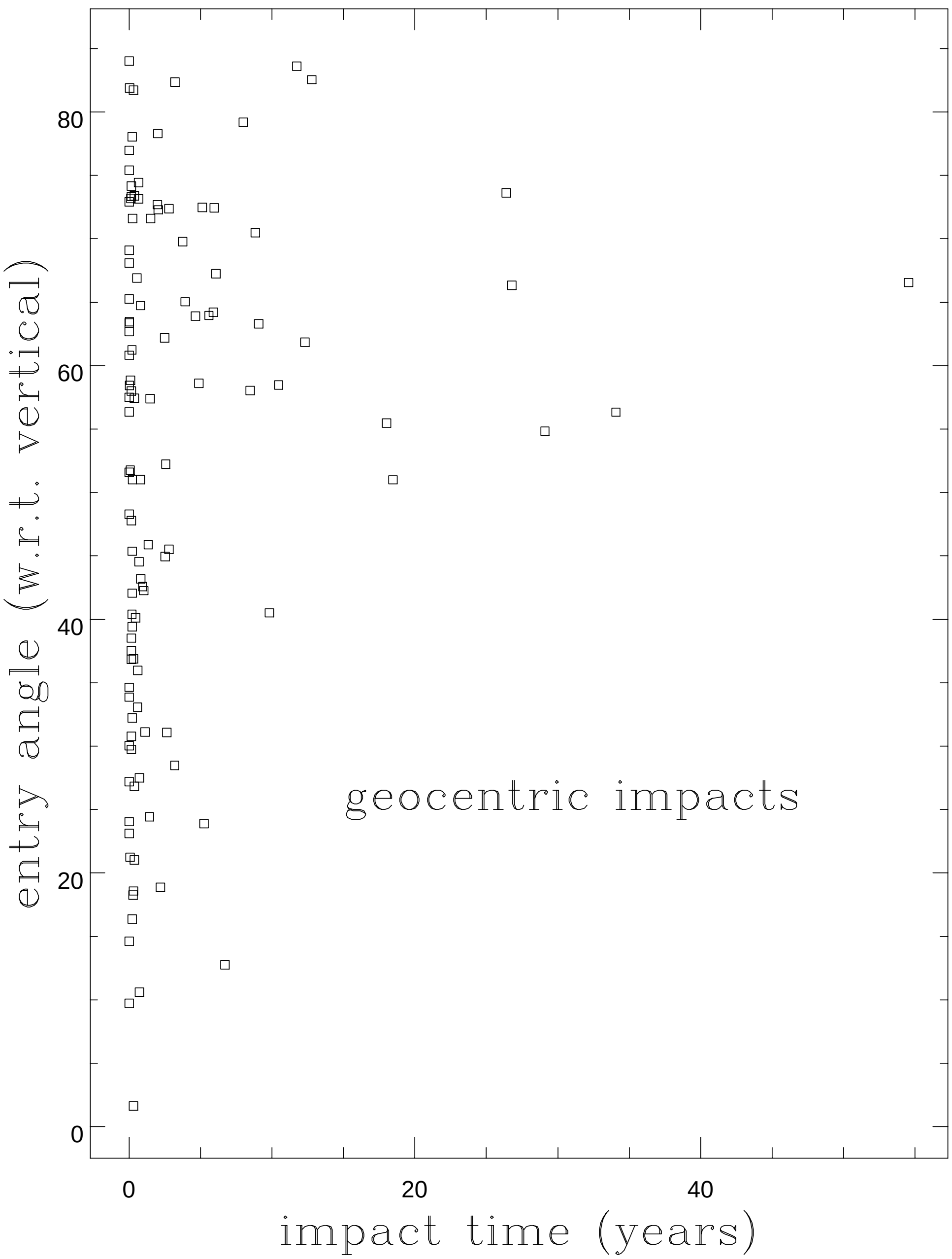

Figure 3.17 Entry angles for the geocentric stage impactors from one of the 2.6 km/s simulations. There is a bias towards entry angles larger than 45^o due to the fact that particles in geocentric orbit are likely to collide with Earth after having their perigees lowered to just below the Earth's surface. This produces a greater likelihood of shallow entries.

One thus concludes that the discovery location on the Earth imparts no information as to where on the Moon a lunar meteorite was launched. Nevertheless Fig. 3.4 demonstrates that objects launched with high velocity (more than 2.6 km/s) have an extreme bias towards coming from the trailing half of the lunar surface *if* those particles are delivered to the Earth without ever escaping geocentric orbit. If the launch-velocity spectrum is flat enough that high-speed particles make up a majority of the escaping ejecta, then geocentric stage deliveries from the leading half of the Moon would be rare. Accordingly, in the absence of other information, the three lunar meteorites with only upper bounds on their CREs (that is, those which might never have been in heliocentric orbit) are somewhat more likely to come from the trailing hemisphere of the Moon. Beyond accepting this very tentative chain of reasoning, one can conclude little. If the 4π CRE of an object could be shown to be only a few days (so that the meteorite arrived via a 'direct' transfer), then one might be able to deduce more, but only if the ejection velocity and angle were known (see Gault 1983). Since such information will not be available, we must conclude that the dynamics can do little to narrow down the source regions of lunar meteorites. In particular, until CREs can be determined to 100-year accuracy, there is little reason to try to distinguish particles that arrived on 'direct' trajectories (transfer times of a few days) from those that conduct many geocentric orbits before impacting the Earth (surviving up to several decades), or even escape to heliocentric orbit and re-impact with the Earth in $< 10^3$ years. Note that if the $v_l \simeq 2.4$ km/s case is the most common (as we might expect), then there are no preferred source regions for either the geocentric or heliocentric stage deliveries.

Any rigorous comparison of the data with simulations like those presented here should attempt to correct for: bias against high entry velocity objects, selection biases in discovery of the lunar meteorites, and biases (due to collisional disruption) against long-lived objects that reach orbits with large aphelia. Construction of a self-consistent model of lunar meteorite delivery, given what is known about the impactor flux, will be the subject of Chpt.6.

3.5 Relevance for the Small Earth Approachers (SEAs)

The Small Earth-Approachers (SEAs) are objects with diameters of 5-50m that have orbits passing close to the Earth. A lunar origin (Rabinowitz 1993) has been proposed for this recently discovered class of objects as a possible explanation for their Earthlike orbits. The simulations performed here are well suited to address the *dynamical* consistency of this hypothesis. I find that the steady-state population after 10 Myr produces a reasonable match to the low-eccentricity component of the SEA population (Rabinowitz 1996) after biasing for telescope detection efficiency and correcting for dynamical protection mechanisms that prevent some surviving objects from entering the observable region (D. Rabinowitz, 1994, private communication). The inclination distribution shown in Fig. 3.9, with very few particles having $i > 30^o$, agrees with the observations. However, too many Aten-type orbits ($a < 1$) are naturally produced, and these are absent in the observed population; this is addressed by Bottke *et al.* (1996), who for this reason claim that martian ejecta supply a better match to the SEA observations.

Perhaps an even more compelling argument against a lunar origin for the SEAs is as follows: The number of SEAs observed so far imply a very large population of SEAs ($\sim 10^{8-9}$ objects of 10m diameter exist according to Rabinowitz 1994). Even if the number of low-eccentricity objects (from a lunar origin) is only 5-10% of this population (Rabinowitz 1994), as might be true if the SEAs are the large-size end of a continuously injected population of lunar impact debris, then one would probably expect much greater numbers of recovered lunar meteorites in the available smaller size range. This problem remains even if the SEAs are the remnants of a single large impact event occurring more than a Myr ago (which would now have a low delivery rate of fragments of all sizes to the Antarctic ice sheet). This issue will be quantified in Chpt. 6. Finally, the lunar SEA hypothesis cannot be ruled out on orbital-dynamics grounds, but it may be difficult to produce the required number of large objects self-consistently. In fact, Bottke *et al.* (1996) calculates that only a few hundred 10-m objects would be launched by the 39-km impact crater Harpalus, and craters larger than this are unlikely to have been produced in the last 10-20 Myr.

3.6 Summary

Available lunar meteorite data are consistent with the simple dynamical model of lunar ejection, geocentric escape, and subsequent heliocentric evolution. The qualitative nature of the delivery of lunar material to the Earth is relatively insensitive to the ejection velocity and typical ejection angle, and thus the details of the launch process should not affect the results.

The numerical studies are fully consistent with the predominance of short CREs that are found in the lunar meteorite sample. One finds that roughly one-quarter to one-half of the ejected lunar material is re-accreted by the Earth in 10 Myr, with a large fraction arriving within the first 50 kyr. An Öpik approach to the problem will underestimate the absolute yield of lunar meteorites by a factor of three to twelve. The spectrum of launch speeds seems to be steep enough that ejecta leaving with speeds greater than 3 km/s are rare. I also conclude that the Earth should be uniformly covered with lunar meteorites, and that the discovery location provides no clues as to the source region on the Moon. There are no preferred launch locations on the Moon for Earth delivery either, given current knowledge about the lunar meteorites.